

The production of turbulence near a smooth wall in a turbulent boundary layer

By H. T. KIM,† S. J. KLINE AND W. C. REYNOLDS

Stanford University, California, U.S.A.

(Received 2 December 1970)

The structure of the flat plate incompressible smooth-surface boundary layer in a low-speed water flow is examined using hydrogen-bubble measurements and also hot-wire measurements with dye visualization. Particular emphasis is placed on the details of the process of turbulence production near the wall. In the zone $0 < y^+ < 100$, the data show that essentially all turbulence production occurs during intermittent ‘bursting’ periods. ‘Bursts’ are described in some detail.

The uncertainties in the bubble data are large, but they have the distinct advantage of providing velocity profiles as a function of time and the time sequences of events. These data show that the velocity profiles during bursting periods assume a shape which is qualitatively distinct from the well-known mean profiles. The observations are also used as the basis for a discussion of possible appropriate mathematical models for turbulence production.

1. Introduction

Several previous works have shown that each of the known portions of the non-dimensional mean-velocity profile of the turbulent boundary layer has a characteristic pattern or ‘visual signature’; these patterns are observable (e.g. by use of the combined-time-streak hydrogen-bubble marker technique) and have been recorded by Kline *et al.* (1967, hereafter referred to as I) and by Corino & Brodkey (1969)‡ using other methods. The structures inferred from these visual signatures are as expected in the outer zones of the boundary layer (the wake and log zones, $y^+ > 40$). However, in the inner zones (sublayer and buffer regions, $y^+ \leq 40$) the inferred structure is distinctly different from that suggested by long-term averages of either mean velocity or fluctuations of velocity taken from single-point measurements.

Since the combined-time-streak marker method makes possible measurement of instantaneous velocity profiles§ over a finite area, it has been used in the present study to examine in more detail the inner-layer structures observed earlier. The

† Present address: APED Department, General Electric Co., San Jose, California.

‡ The dissertation of Kim (Kim *et al.* 1968*a*) was prepared before the authors were aware of the work of Corino & Brodkey; the two works provide independent complementary information.

§ We emphasize here that this marker method, unlike most others gives *both* a general qualitative pattern and quantitative data on velocity.

earlier studies showed that the flow pattern in the inner layers consists of longitudinal 'streaks' of slow- and fast-moving fluid side by side. This structure is apparently universal in the inner layers of turbulent shear flows near smooth walls. Its major length and time scales have been measured by Runstadler, Kline & Reynolds (1963) for $dp/dx = 0$ and for accelerating and decelerating layers by Schraub & Kline (1965); these results have also been summarized in I. Independent confirmation of the length scales involved has now been given by Bakewell & Lumley (1967) and Coantic (1967) from hot-wire data, and of the visual signatures in the inner layers by Clark (1968). Black (1966) has suggested a relation between the time scales and the wall-pressure fluctuations measured by many other observers at low Reynolds numbers. Thus the existence and universality of this structure for smooth walls† seems well established. The only major residual doubt appears to be the extrapolation of the scaling to high Reynolds numbers (see below). However, the implications of this structure as they affect the dynamics of the motions are still very properly the subject of varying interpretations. The central purposes of the work reported herein are to report new data on this inner-layer structure, and hopefully, to further clarify its interpretation. The relation (if any) between the inner-layer structure and the production of turbulence near smooth walls is given particular attention.

Runstadler *et al.* (1963) hypothesized that the production of turbulence in the inner layers was largely due to the bursting‡ of the observed flow model, and more particularly to the eruptions of the low-speed streaks.§ They further hypothesized that this bursting process in a certain sense dominated the energy transfers in the entire turbulent shear layer. As already stated, it is the first part of this hypothesis that the present work examines in more detail. The second part, the relation between the inner and outer layers, will be discussed separately elsewhere.

In examining the relation between bursting and the production of turbulence, three questions are treated. First, and most essential, what fraction (if any) of the turbulence production in the inner layers is actually associated with the 'bursting' process. Second, what are the details of the flow processes leading to and during 'bursting'. Finally, the nature of the process and the implications for theoretical advance and future experimentation are discussed. The first two matters are reports on new data; the third is more speculative.

A shift in nomenclature from that used by Runstadler *et al.* (1963) and I is employed here. Since we concern ourselves with describing the stages of the bursting process, it becomes necessary to define the various stages distinctly from the whole. Accordingly, we now use the term 'bursting' to mean the entire process which carries the flow from a relatively quiescent wall-model structure to a more random chaotic turbulent character. We divide bursting into three stages; the

† The rough-wall case is not entirely the same; see, for example, Liu, Kline & Johnston (1966).

‡ Nomenclature altered slightly from previous references; see below.

§ It must be emphasized that it is not the existence of the low- and high-speed streaks, but rather the 'bursting' of the low-speed streak that is believed associated with production of new turbulent kinetic energy. This point has apparently occasionally been misread.

last of these stages we call 'breakup'. Thus, in the present description, it is essential to distinguish between bursting, the overall process, on the one hand, and breakup, the third and last stage of bursting, on the other. In previous discussions, this distinction is not made, and the two words are used more or less interchangeably.

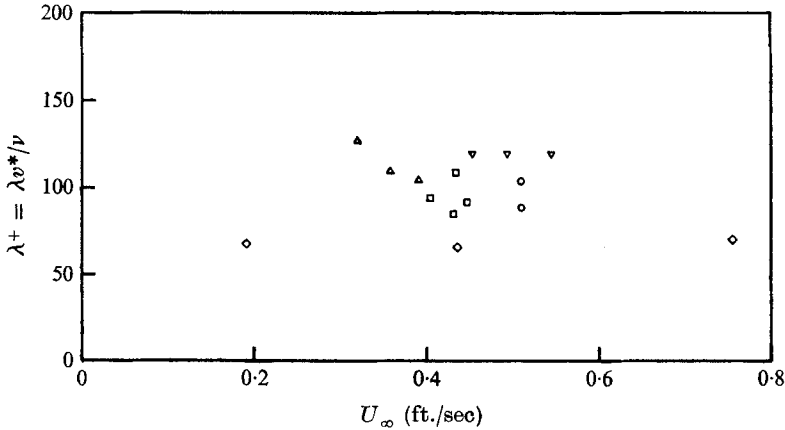


FIGURE 1. Non-dimensional transverse streak spacing in viscous sublayer, λ^+ , as a function of free-stream velocity for flat plate flow.

- | | | |
|-------------|----------------|---------------------------------|
| \diamond | $dp/dx = 0$ | Runstadler <i>et al.</i> (1963) |
| \circ | $dp/dx = 0$ | } Schraub & Kline (1965) |
| \triangle | $dp/dx \geq 0$ | |
| \square | $dp/dx > 0$ | |
| ∇ | $dp/dx > 0$ | |

2. Brief recapitulation of previous results

In figure 1, the major length-scale correlation of the streaky structure of the inner layer is reproduced. It should be noted that the *mean* transverse length scale appears to correlate well on the wall-layer length parameter ν/v^* . In figure 2, the correlation of the *mean* burst rate for the flat plate flow is given. As will be shown later, the time scale corresponding to the burst rate, i.e. the *mean* time between bursts in the present notation, appears to correlate well when normalized on the wall-layer scales (that is, the characteristic time ν/v^{*2}). However, individual measurements of both length and time scales vary significantly from the mean; in both cases the ratio of the standard deviation of individual readings to the mean reading is of the order of 0.4. Hence, one must think of a dominant band of length (or time) scales rather than a single sharply defined value. Moreover, bursting rate is a strong function of pressure gradient; see I, figure 16(b). Also, the range of Reynolds numbers, R_θ , in these data is quite restricted; important comment on R_θ dependence is given in §5, see figure 24.

The observations of Runstadler *et al.* (1963), Schraub & Kline (1965), Meyer & Kline (1962), and numerous other experiments including those in the film 'Flow Visualization' (Kline 1963), all confirm the fact that the streaky wall model is always found from the first existence of a turbulent spot (Emmons 1951)

wherever the flow is turbulent on a smooth wall, and that the length scales are consistent with figure 1 wherever clear measurements are available. Regarding correlations of the time scales, see also §5. The results of various workers on transverse scale, λ^+ , are summarized in table 1.

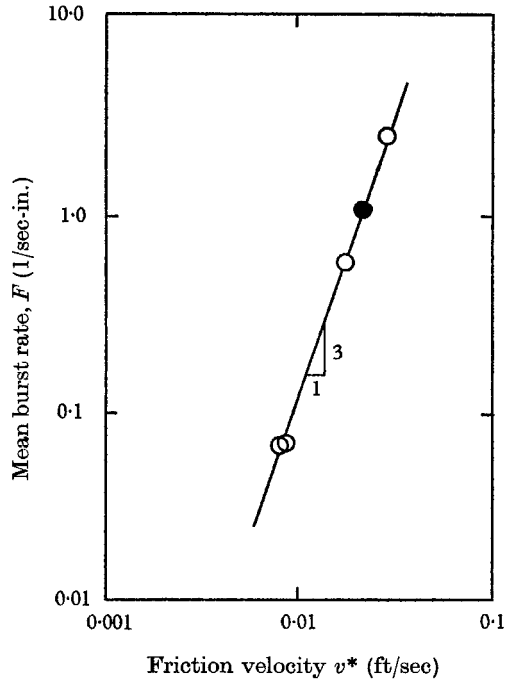


FIGURE 2. Mean time between bursts as a function of friction velocity for flat plate at a moderate and relatively constant R_θ ; see also figure 24. \circ , $dp/dx = 0$, Rundstadler *et al.* (1963); \bullet , $3x$ stations, Kline *et al.* (1967).

The flow pattern in the region near the wall always consists of low- and high-speed streaks. Except in adverse pressure gradients, the low-speed streaks always move slowly downstream with the mean motion near the wall, and also very gradually migrate outward away from the wall. When they reach a distance sufficiently far from the wall they begin to oscillate and finally break up. The location of the low- and high-speed streak pattern is not fixed by a given tunnel; indeed, Schraub & Kline (1965) showed the pattern to be random in the sense that streak location approaches closer and closer to a uniform distribution over the wall area when observed for long times. Kline & Runstadler (1959) also showed that a continual interchange between the fluid very close to the wall ($y^+ = 0.01$ and less) and the outer layers is observed when the dye traces are followed for a sufficiently long downstream distance. The dye initially very near the wall is found farther and farther from the wall as it is followed downstream; if another colour of dye is introduced farther downstream, then the wall-layer streaky structure is observed in the new dye colour but closer to the wall. These 'new' streaks again have the length correlation of figure 1.

In summary, all available indications tend to confirm the universality of the streaky structure in the inner layers of turbulent boundary layers on smooth surfaces.

Reference	U_∞/ν (1/ft)	R_x (or R_D)	R_θ	Max λ^+	Method and substance
Coantic (1967)	5.92×10^3	5×10^4	2500	110–130	Hot-wire, averaged correlations, air
Willmarth <i>et al.</i> (1966)	1.29×10^5	—	40 000	200	Wall press, averaged correlations, air
Runstadler <i>et al.</i> (1963)	4.4×10^4	(0.2– 0.8) 10^5	2000	100 ± 20	Boundary layers, visual, dye and H ₂ bubbles, water
Schraub & Kline (1965)					
Kim <i>et al.</i> (1968 <i>a</i>)					
Bakewell & Lumley (1967)	9.34×10^3	8.7×10^3	≈ 1877	≈ 100	Averaged correlations, hot wire, glycerine and water
Clark (1968)	$\sim 4-5 \times 10^4$	$\approx 30\,000$	—	$\times 100$	Channel flow H ₂ bubbles visualization, water
Gupta (1970)	$2-6 \times 10^4$	—	2000– 6500	≈ 95	Air, short-duration correlations from multiple hot wires

TABLE 1. Measurements of $\lambda^+ = \lambda v^*/\nu$, where λ is the mean inner streak spacing. Typical conditions shown; — means unknown or irrelevant to flow condition

3. Experimental procedures

All results reported here were taken from two flows in an open surface water channel of width 3 ft and depth 10 in. The two-dimensionality of the flow is relatively good, as shown in figure 3. The free-stream turbulence level is $(\overline{u^2})^{1/2}/U_\infty = 1-2\%$. Details of the apparatus and the flow are reported in I and the underlying reports, and are not repeated here. Since the objective of the study was a detailed investigation of flow models, only two flows were studied but each in much more detail than in prior work. Both are flat plate flows with zero pressure gradient but with U_∞ approximately 0.25 and 0.50 ft/sec, respectively. The important boundary-layer parameters for the two flows are included in table 2.

In this study, two measurement methods have been used: the combined-time-streak marker method using hydrogen bubbles, and constant-temperature hot-wire anemometer measurements combined with dye injection at the wall. The techniques of the hydrogen-bubble method are given in detail by Schraub *et al.* (1965). The basis for the hot-wire anemometer is described by Sabin (1963), but the unit employed incorporates improvements described in part by Uzkan & Reynolds (1967); these instrument details will be reported separately. The only new technique in the work is the combined use of two perpendicular bubble wires with split image views in what is called a dual view. See figure 4 below for axes

and views. As shown in figure 4, different terms are adopted to delineate between the camera viewing direction and the direction of the marker wire.

It would have been very useful to use the hot-wire simultaneously with the bubble method. This has, so far, not proved feasible owing to failure of the hot-wire element when the bubble current was pulsed. This problem is under further cur-

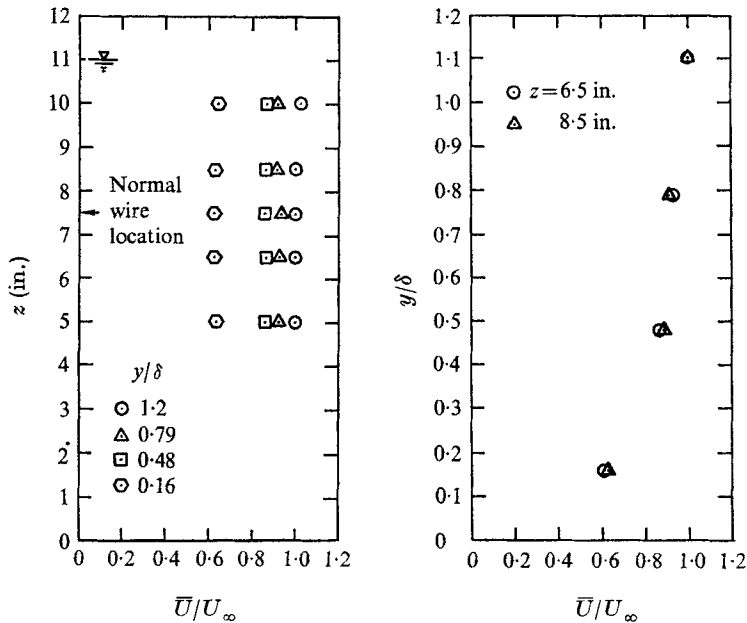


FIGURE 3. Mean velocity profiles at working section illustrating degree of two-dimensionality.

U_{∞} , ft/sec	0.25	0.50
$\delta_{0.99}$, inch	3.1	3.0
δ^* , inch	0.54	0.41
θ , inch	0.372	0.31
$H = \delta^*/\theta$	1.45	1.32
v^* , ft/sec	0.012	0.0234
R_x	(3.4) (10^5)	(6.2) (10^5)
R_{θ}	666	1100

TABLE 2. Summary of boundary-layer parameters which describe experimental flow condition tested

rent study, but success with this combination has, to date, not been achieved, and hence a combination of injection of dye at the wall and hot-wire measurements was used instead. In using dye injection, care was taken to adjust injection pressure so that excessive disturbances were not created.

With regard to the bubble observations, two things should be kept in mind. First, it is possible to make measurements of the *instantaneous* velocity profile. By comparisons of these instantaneous profiles with the mean profile, values of fluctuations in velocity can also be obtained. This, in turn, allows calculation

of values of instantaneous contribution to the turbulence production. All these data can also be linked to the observed visual patterns. The accuracy of these data, particularly of fluctuations, is low, but no other known method offers combination of all these results. Indeed, as will be seen, the ability to observe instantaneous as opposed to mean velocity profiles appears to be crucial in gaining understanding of the nature of turbulence production in this case.

	Marking wire direction	View (line of sight of camera)
y	Normal	Plan
z	Transverse	Side

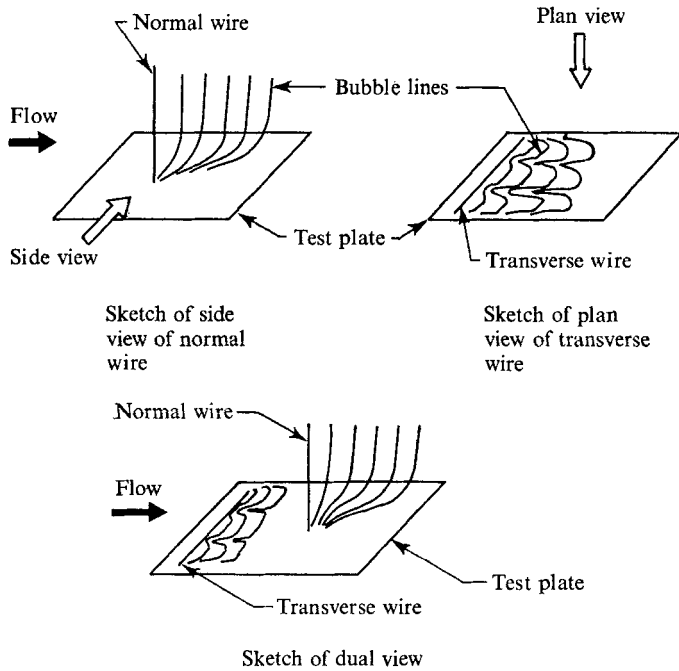


FIGURE 4. Orientation and nomenclature of bubble wires and camera views.

Moreover, the bubble measurements are an excellent complement to hot-wire measurements in several ways since each does relatively well what the other does poorly. As already noted, the bubble measurements have both a quantitative and qualitative output, and both kinds are reported herein. In the discussion that follows, the qualitative results are mostly illustrated by pictures, but a few results are based on 'direct observation by eye'† since it was not possible to successfully reduce to two dimensions certain aspects of the four-dimensional time-space flow patterns observed. The number of instances in which the reader is thus asked to take the word of the reporting observer is, however, held to an absolute minimum, and these instances do not in any way affect the central

† See Kim *et al.* (1968*a*).

quantitative results since they provide information only about certain qualitative details.

4. Description of overall behaviour of flow model during bursting

In this section a number of new details of the wall-layer flow model are described via still pictures and word descriptions in order to provide an overall understanding of the flow model. Quantitative measurements relating the flow models to significant flow dynamics and energy terms are given in the next section. Since still photographs do not convey as much information as motion pictures in a complex transient flow pattern such as that recorded here, a companion motion picture has also been prepared (Kim *et al.* 1968*b*).

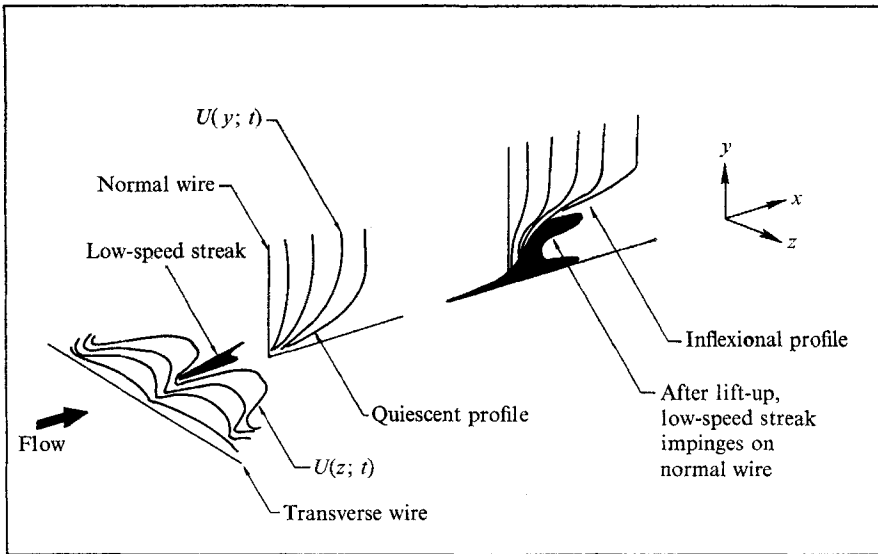


FIGURE 5. Sketches of the typical lift-up stage of a low-speed streak during the bursting process.

The total process of 'bursting' is a continuous chain of events leading from a relatively quiescent wall flow to the formation of relatively large and relatively chaotic fluctuations. The process, in the cases observed, is of an on-off or intermittent character. We describe the bursting process in three somewhat arbitrary parts for purposes of clarity.

The first stage of bursting is the lifting of a low-speed streak from the wall. As the low-speed streak moves downstream it also gradually moves away from the wall. The observed secondary (streamwise) vorticity embodied in a low-speed high-speed streak pair initially is very low. As a result, the low-speed streak at first moves away from the wall very slowly over a very long streamwise extent. One might say that its outward motion, away from the wall, is then the cumulative effect over long distances (or times) of a small streamwise vorticity. However, once the low-speed streak has reached some critical distance from the wall, it appears to turn much more sharply outward, away from the wall, but still moving

downstream. This more rapid outward motion we call 'low-speed-streak-lifting' or, for brevity, 'streak-lifting'. The use of the words 'critical distance' should not be interpreted as sharply defined single distance; there is, in fact, a distribution of critical values when measured over a large number of streak-lifting processes; see below. The early slow lifting and subsequent more rapid outward motions are sketched in figure 5.

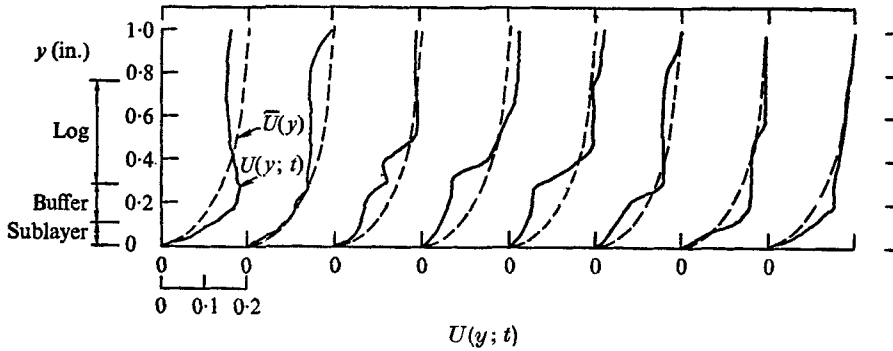
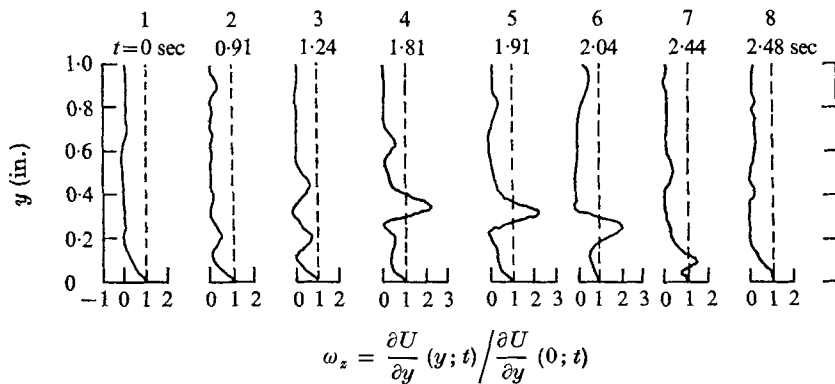


FIGURE 6. Comparison of instantaneous velocity profiles, $U(y; t)$, with the mean profile $\bar{U}(y)$ over a typical bursting cycle.



$$\omega_z = \frac{\partial U}{\partial y}(y; t) / \frac{\partial U}{\partial y}(0; t)$$

FIGURE 7. Instantaneous vorticity profiles, $\omega_z(y; t)$, normalized on wall value, $\partial U/\partial y(0; t)$, over a typical bursting cycle.

When a low-speed streak lifts, it carries with it, away from the wall, fluid particles of very low relative speed; the relatively rapid outward motion thus creates a narrow inflexional zone containing two reversals of slope-gradient and an inflexion point in the instantaneous velocity profile. This creation of an inflexional zone is clearly visible in the example of figure 6 and it is distinctly typical of all bursting processes observed. It should be emphasized that, while the instantaneous inflexional profile often leads to a growing oscillation and breakup, it does not always do so. This implies that the nature of the growth and breakup of oscillations requires further study. Moreover, the inflexion point

occurs at a point of maximum vorticity as shown in figures 6 and 7 where instantaneous profiles of both velocity and streamwise vorticity, † ω_z , are shown for a sequence of times during which bursting starts and ends. Such an inflexional velocity profile is inviscidly unstable, in steady flow, to disturbances within a finite band of frequencies. A similar (Kelvin–Helmholtz) instability also occurs in free shear layers of most types; however, there is an important difference between the two cases. In the free shear layers the *mean* profile contains an inflexion point; in the flat-plate boundary layer studied here, the inflexional profile occurs only at some instants when the profile is strongly perturbed by the lifting of a low-speed streak.

To make clear the nature of the instantaneous profiles for the flat-plate flow, we now contrast two cases as seen in the dual views. Note that in the dual view used (see figure 4), the transverse bubble wire is located upstream of the normal bubble wire; the amount of streamwise separation is selected so that a maximum of low-speed streaks made visible at the transverse wire will be ‘lifting’ near the normal wire. However, the low-speed streak at lifting is thin; its transverse extent is of the order of $10 < z^+ < 30$ compared to a total mean wavelength of $\lambda^+ = 100$.

The normal wire has negligible z extent, and hence most low-speed streaks pass by the normal wire ‘out of plane’ even when they originate in the zone given by a λ^+ extent of 50 to either side of the location of the normal wire. Thus at any instant there are two possibilities: (i) a lifted low-speed streak passes over the normal wire, (ii) all existing lifted low-speed streaks pass out-of-plane from the normal wire. In the first case, when a lifted low-speed streak passes over the normal wire, then inflexional profiles are observed in the time lines generated at the normal wire. In the second case, when no lifted low-speed streak impinges directly on the normal wire, the instantaneous velocity profiles seen downstream from the normal wire appear to have the general shape which is typical of the mean velocity profile – they do not contain inflexion points. ‡

The most significant observation is that the observed inflexional instantaneous velocity profiles are seen to lead to the growth of an oscillatory disturbance just downstream of the inflexional zone. The observed growth of the oscillation is very rapid; it appears to reach a relatively large scale within one or two cycles of oscillation.

The oscillatory motion is at first quite regular, and the entire motion seems to remain quite ‘organized’ for 3–10 cycles. However, after 3–10 cycles, a more random chaotic motion appears in the marked time lines. This more chaotic motion we call ‘breakup’ in this discussion; it is the third and final stage of the bursting process. As in the passage from low-speed streak to lifting, there is no sharp demarcation between the second and third stages; they are made separate only for clarity in description.

The onset of ‘breakup’ signals the return of the instantaneous profile to a

† In this flow ω_z is taken as $\partial U/\partial y$ since it is large compared to $\partial V/\partial x$. The total velocity U is the sum of \bar{U} and u .

‡ We presume local inflexion profiles exist at such times in other locations ‘out-of-plane’ to the normal wire; they are not marked by bubbles, and hence are not visible, however.

shape qualitatively like that of the mean profile, including the vanishing of the inflexional zone. Dye traces in side view frequently show a movement of the low-speed streak back towards the wall during these times; the cycle of the intermittent process is thus completed, and will in due course start again.

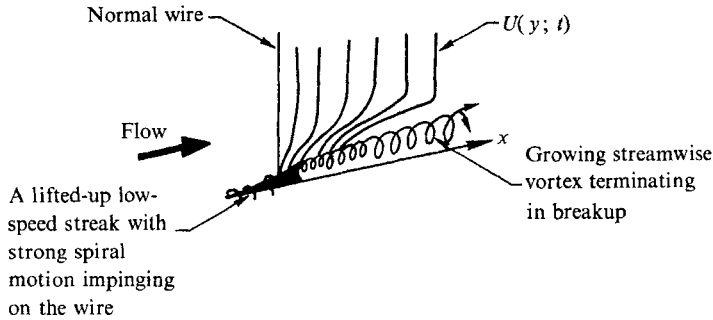


FIGURE 8(a). Schematic illustration of the formation of streamwise vortex motion during bursting.

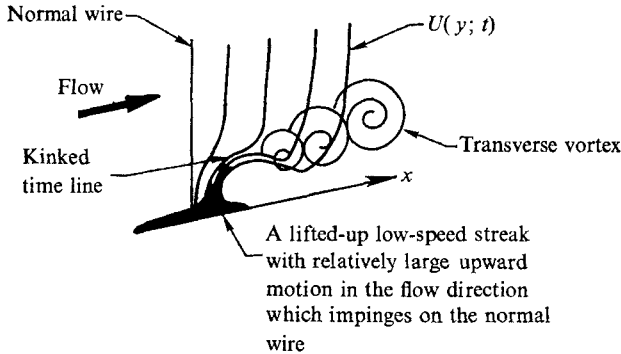


FIGURE 9(a). Schematic illustration of the formation of a transverse vortex during bursting.

We turn back now to a more complete description of the oscillatory growth motion or second stage of bursting. The dominant mode appears to be a streamwise vortex motion in which the vortex size grows and its strength increases as the motion proceeds downstream as illustrated in figure 8(a). Dye traces of this motion show oscillation in both plan and side views; see particularly Runstadler *et al.* (1963). However, dye visualization does not reveal the strongly vortical nature of the flow. The finer-grained bubble pictures show clearly that a vortical motion is involved; see, for example, marked sections in figures 8(b) and (c) (plate 1). Again, these are typical of a large number of photos. The two less common modes of oscillatory growth involve respectively: (i) a 'transverse-vortex' and (ii) a repeated oscillation or what we call, for lack of a better name, 'wavy motion'. The transverse vortex mode is shown in figures 9(b)–(f) (plates 2–4); it is relatively rare. The wavy motion case is somewhat more common; it appears much as if the on-off process repeats several times very rapidly. An example is shown in figures 10(d)–(j) (plates 5–8).

No counts of frequency of the three modes have been made, but probably in excess of two-thirds of the cases involve the streamwise vortex mode.

In summary then, the overall model of bursting can be described by the following three stages: (1) Slow lifting of a low-speed streak accumulates until a shift occurs involving more rapid outward motion of the low-speed streak; at this time,

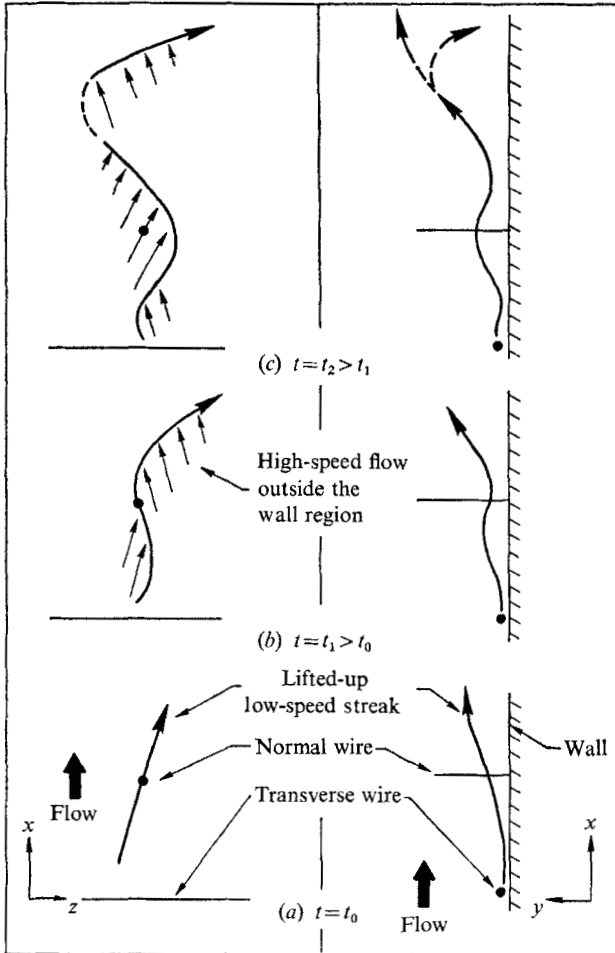


FIGURE 10(a)–(c). Schematic representation of ‘wavy mode’ second stage of bursting. (b) Inflexional profile near intersection of line through A with zone B , $t = t_0$. (c) Kinked time lines near the intersection of line through C with zone D . This is incipient formation of transverse vortex. $t = t_0 + 0.37$ sec.

an inflexional *instantaneous* velocity profile is observed. (2) Downstream from the inflexional zone rapid growth of an oscillatory motion is observed; it continues for a few cycles. (3) The oscillation is terminated by the onset of a more chaotic fluctuation called ‘breakup’. This completes the cycle, and the velocity profile returns to a form generally like the mean profile shape. These general processes are observed in all cases studied; the details are uniform up to the end of the first

stage, low-speed-streak-lifting, but the second and third stages vary from case to case in structural detail.

So far, we have refrained from interpreting these observations. We make here some remarks, purposefully held distinct, in this regard. The uniformity of the observation of inflexion points in the instantaneous profile, prior to growth of an oscillation, tends to substantiate the hypothesis advanced earlier (I) that the breakup of the wall model is due to a local intermittent instability. The termination of the oscillatory growth by more chaotic motions is of course highly suggestive both of a secondary instability and of the passing of fluctuations along the wave-number scale to higher frequencies and smaller motions. Thus it appears plausible to associate the oscillatory motion of stage (2) with turbulence production and the more chaotic breakup of stage (3) with wave-number transfer. There are, however, no direct data on these points thus far; the pictures are merely suggestive.

It is also worth noting that stage (2), the oscillatory growth, starts with a scale given by the y and z extent of a lifted low-speed streak; this is typically $10 \nu/v^*$ to $30 \nu/v^*$; it is not as much as $50 \nu/v^*$ because the extent of low-speed streaks at $y^+ = 10$ is already less than that of the high-speed streaks (Schraub & Kline 1965) and further 'thinning' is observed in the lifting process. The total boundary-layer thickness in these observations is roughly $800 \nu/v^*$. During the oscillatory growth, scales of motion often grow to half the boundary-layer thickness, that is to the order of $400 \nu/v^*$. Thus the scale increases at least one order of magnitude during the oscillatory growth process, and this occurs in a very short streamwise distance; see, for example, just upstream of the zones marked B and D on figure 8(b) and (c). One might argue that this same observation could arise from the entrainment of the lifted low-speed streak by a 'large eddy'. The pictures, however, argue against this view in that they show the process to be so clearly intermittent, so abrupt in on-off characteristics, and, more important, to uniformly follow only from an inflexional instantaneous velocity profile. Finally, in one case a calculation has been made of the unstable frequencies of the actual instantaneous velocity profile using a simple model. The model is a numerical solution of the Orr-Sommerfeld equation using the measured instantaneous velocity profile as the mean profile. The oscillation frequency and its growth rate observed during the bursting period are in reasonably good agreement with the unstable disturbances as calculated using this model (Kim *et al.* 1968*a*). Figures 11 and 12 compare Reynolds stress and the fluctuations of the Orr-Sommerfeld wave, \bar{u}^2 , near the wall which were calculated from the model with the fluctuations observed during the bursting period. It is seen in these figures that location of peak and trend of variation of the distributions are in adequate agreement. The quasi-steady model is quite crude; nevertheless, the agreement between the calculated and observed values again strongly suggests that an instability is involved.

No quantitative investigation was made of the kinematics or dynamics of the obviously increased vorticity observed in the streamwise vortex mode of stage (2) of bursting. Visual observations of the flow suggest that vortex stretching is involved; however, the stretching appears to be along the arms of the vortex loop and not at the loop head as suggested by Stuart (1965) in connexion with

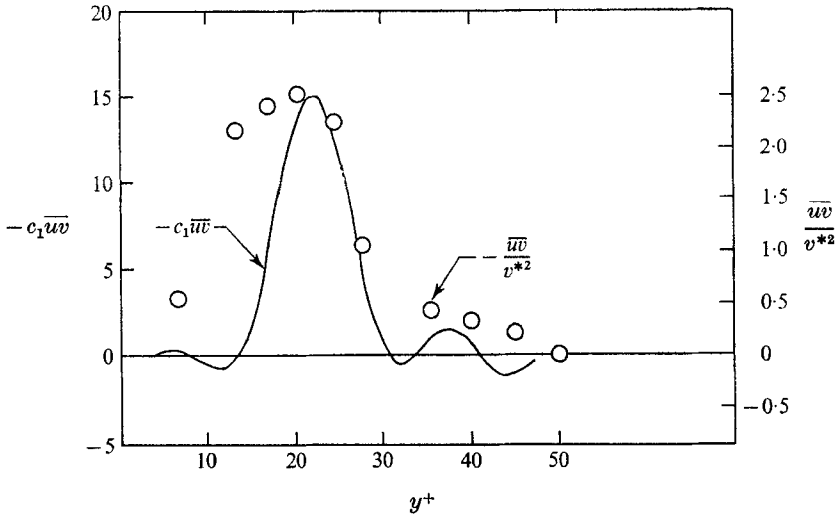


FIGURE 11. Comparison of the form of the Reynolds stress measured from H_2 bubble data during a bursting period with calculations using two-dimensional steady linearized equations (Orr-Sommerfeld). Scales are arbitrary. \circ , Burst period data, $t = 0.67$ sec; —, two-dimensional lines theory.

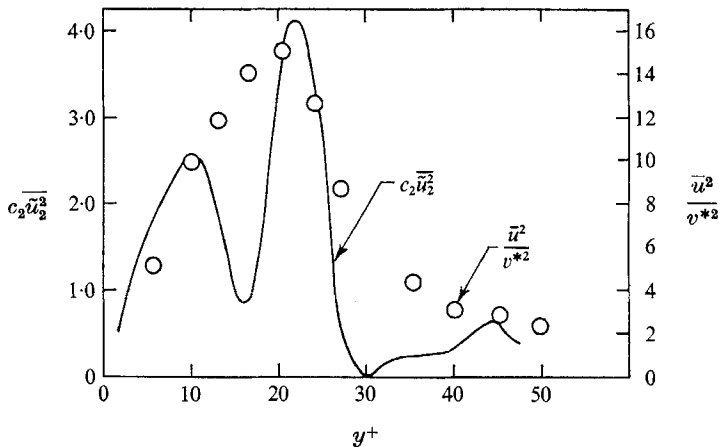


FIGURE 12. Comparison of the form of the organized fluctuation $\overline{u_2'^2}$ measured from H_2 bubble data during bursting with calculations using two-dimensional steady, linearized equations (Orr-Sommerfeld). Scales are arbitrary. Symbols same as figure 11.

laminar-turbulent transition. Moreover, the dynamics cannot be due to inviscid vortex stretching alone since in that case an increase in vortex radius requires a decrease in rotation to preserve circulation. In the films of the streamwise vortex mode it is very clear that a considerable increase in diameter occurs simultaneously with very rapid increase in rotation speed.† Thus some kind of energy is being transferred to the vortex, and probably at a rather high rate; the source of this energy exchange has not been investigated. M. Lawson has also suggested to the authors that the visual analogy between the vortex breakdown photographs and

† See film (Kim *et al.* 1968b).

those of Runstadler *et al.* (1963) suggests that the breakup is brought on by vortex breakdown. However, no data on these points are available in the present study, nor in any other study yet known to the authors; these intriguing questions remain open for the present.

The observations of Corino & Brodkey (1969) are for pipe flow, and they use different observational techniques and descriptive terminology. Despite these differences we believe their observations are essentially consistent with those presented herein and by Kline *et al.* (1967).

5. Data relating flow models, dynamics and energy processes

To establish relations between flow models and dynamics in this complex intermittent flow field it was first necessary to establish a suitable sample. This was attempted by forming the ensemble average of a large number of instantaneous profiles (about 800). We then investigated the number of samples required to give an ensemble average agreeing with the measured mean profile (from hot-wire data) within the uncertainty of the mean data at an estimated confidence level of 0.95. It was hypothesized that data runs long enough to give a correct mean profile would provide good samples. For the most part this is true, but one exception was subsequently found and must be mentioned.

As will be seen in the data that follow, the longest time scale in the entire field is the 'time between bursts', that is the mean time between beginning of one bursting cycle and beginning of the next. Moreover, the variation of time between bursts from sample to sample is large. As a result, the time used was not long enough to average over bursting processes with high accuracy. Fortunately, this does not prejudice the central results that follow, and since the work involved in the procurement of these data took a long time, they were not repeated. We did not expect this difficulty, so we mention the problem here both so that the data can be properly understood, and for the benefit of future workers. As will be seen, related difficulties have also distorted some past results by other workers using statistical techniques.

The central question here is whether the bursting process is related to all or a large part of the turbulence production near smooth walls. To answer this question a special parameter is defined as follows:

$$\alpha = \lim_{T \rightarrow \infty} \frac{1}{T} \int_0^T \alpha_\beta P(t) dt \bigg/ \lim_{T \rightarrow \infty} \frac{1}{T} \int_0^T P(t) dt,$$

where $P(t)$ is the instantaneous contribution to the mean turbulence production rate, T is the time interval of sampling discussed above, t is time, and α_β , the burst intermittency factor, is defined to be one during bursting periods, but zero for all other times in the range $0 \leq t \leq T$. Under these definitions, α is the fraction of turbulence production during all bursts for the total time studied. Also, we note that the denominator is the mean turbulence production rate:

$$\bar{P} = \lim_{T \rightarrow \infty} \frac{1}{T} \int_0^T P(t) dt.$$

$P(t)$, the instantaneous contribution to the mean production, is $-u(t)v(t)\partial\bar{U}/\partial y$.

The question concerning us can then be stated as follows: Is α large compared to the fraction of the total time period occupied by bursts, γ , where γ is defined below?

$$\gamma = \lim_{T \rightarrow \infty} \frac{1}{T} \int_0^T \alpha_\beta dt.$$

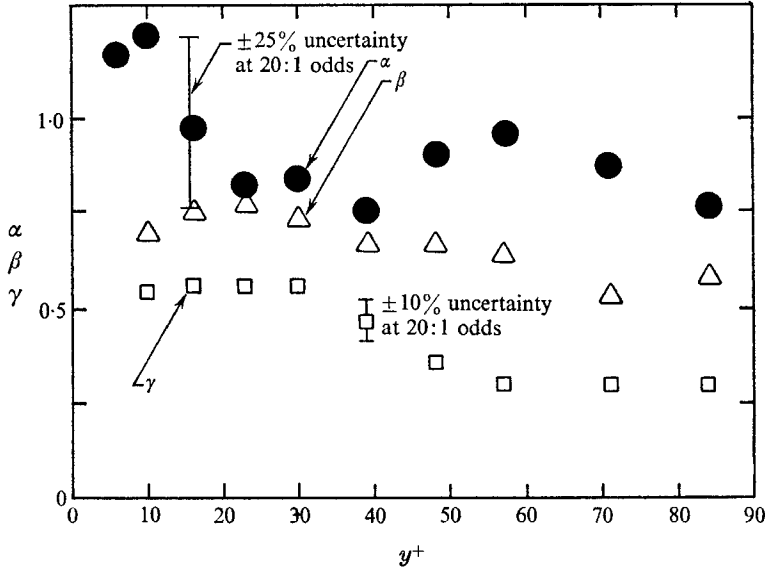


FIGURE 13. Fraction of turbulence production, α , fraction of one-dimensional mean-square turbulent energy, β , and fraction of occurrence time for bursting periods, γ vs. y^+ . Results from H_2 bubble data; all bursts during observed sample taken into account.

The results for flow with $U_\infty = 0.25$ ft/sec are shown in figure 13. Figure 13 shows that the answer to the above question is an unequivocal 'yes'; essentially all the turbulence production in the zone $0 \leq y^+ \leq 100$ does occur during bursting, and little or no production occurs on the average during non-bursting times.† Some comment is however required on figure 13. First, it must be noted that the uncertainty in P is large. The controlling uncertainty in P arises from the measurement of transverse fluctuations velocity, v , and the resulting uncertainty in P is estimated at $\pm 25\%$ using 0.95 confidence level. Thus neither the upward nor downward variations of α from 1 can be considered as entirely conclusive; it can only be said that essentially all the production does occur during bursting times. The values in excess of 1 are not necessarily in error, however. To obtain $\alpha > 1$ at given y^+ merely requires a mean negative Reynolds stress during non-bursting times, and as we have noted in the preceding section, one does see the motion of low-speed streaks toward the wall and a lessening of fluctuation level during these periods. The location of the very high values in the zone of maximum turbulence production as measured by others (Klebanoff 1956; Laufer 1954), and the strong similarity of the curves for the two cases measured also argue for the reality of the existence of values of α in excess of 1; however, the question cannot be decided by the present data.

† Data are limited to $y^+ < 100$; same mechanism likely for $y^+ > 100$.

A further check on the association between production and bursting, in particular the second or oscillatory growth stage, is shown in figure 14. Figure 14 compares a histogram of the locations of the oscillatory growth stage of motion with the production data of Klebanoff (1956) in wall-layer co-ordinates. The histogram was constructed by marking off cells of equal y^+ extent of the size shown on the figure, and counting when oscillatory growth was observed within each cell. When the oscillatory growth motion was in more than one cell, it was counted as present in all of them. The peaks of the two curves were rescaled to the same height in the figure for ready comparison. The agreement of the shape of the two curves is indeed strong evidence of the association of the processes, particularly in view of the very odd shape of the production curve.

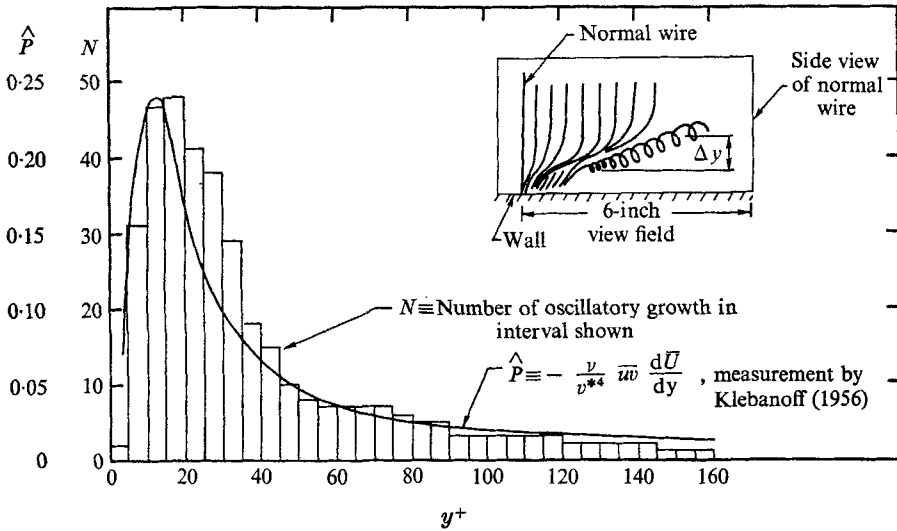


FIGURE 14. Shape of the non-dimensional turbulence production, $\hat{P}(y^+)$, from the data of Klebanoff (1956), compared to the shape of the histogram of burst frequency occurrence $N(y^+)$.

Figure 15 shows two portions of a long run of hot-wire, output indicating u , taken just outside the sublayer. On these signals two zones are indicated by arrows. These are periods which the associated dye pictures showed to be bursting times. For comparison, the oscillatory growth frequencies are again shown. It is seen that the characteristic signature of the bursting time is the very rapid start-up (usually in less than two cycles, and often in less than one) of a large oscillation at the frequency of the oscillatory growth motion. At the ends of bursting time, the oscillation stops just as abruptly. Once this has been observed, some degree of order can be seen in traces which otherwise appear entirely without organization; this again emphasizes the great utility of combined visual and quantitative techniques in flows of this complexity. The very abrupt on-off nature of the record and also the agreement of the observed frequencies and growth rates of the oscillation during bursting time with those of the unstable disturbances computed for the measured instantaneous velocity profile both constitute evidence in favour of the local instability concept. Related but more

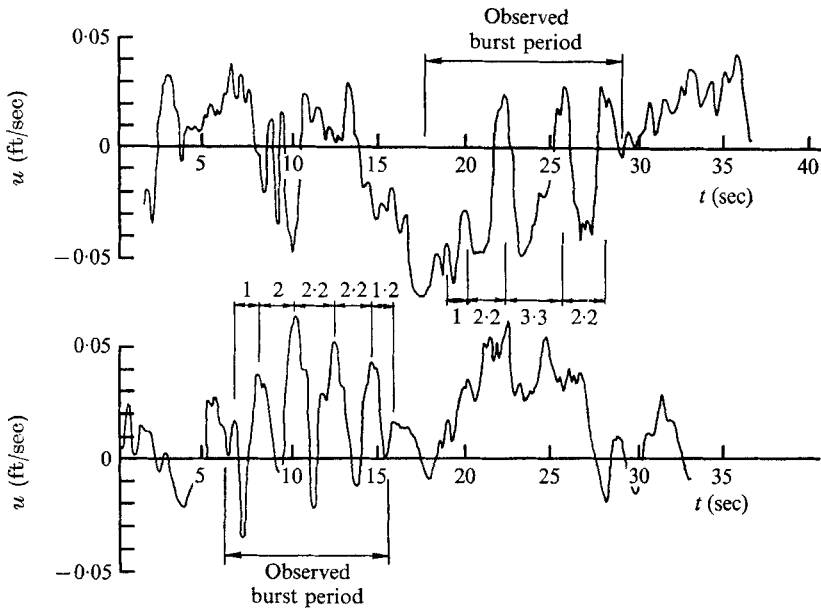


FIGURE 15. Two velocity fluctuation samples, $u(t)$, contrasting the characteristics of bursting and non-bursting times.

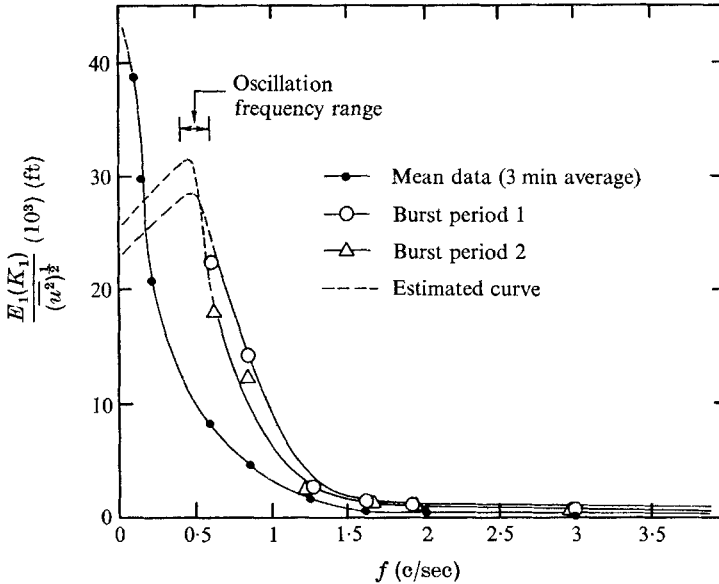


FIGURE 16. Comparison of normalized one-dimensional spectra $E_1(k_1)/(\overline{u^2})^{1/2}$ for long and short averaging times. Hot-wire data; $U_\infty = 0.25$ ft/sec., $y^+ = 15$. $(\overline{u^2}_{\text{digital}})^{1/2} = 0.0267$ ft/sec; $(\overline{u^2}_{\text{analog}})^{1/2} = 0.027$ ft/sec.

refined studies of this type capitalizing on the experience gained here would seem to be very desirable.

Figure 16 shows two short-duration one-dimensional energy spectra of u -velocity fluctuation taken respectively for the two bursting periods shown in figure 16 and also for an entire 3 min long sample. These were obtained with a Quantech 304 wave analyzer in the analog mode using sweep times considerably less than the extent of the bursting interval or quiescent time. It can be seen that an increase in total turbulent kinetic energy occurs during the bursting times, but that most of this added energy is in the frequency range near the observed frequency of oscillatory growth which is marked on the figure (see both figures 15 and 16). It can be seen that these frequencies are in the centre of the high energy range of the turbulent fluctuations, again reinforcing the idea that while the bursting process is the overall production, the primary energy transfer occurs in the oscillatory growth stage. Looking back also at figure 13, one observes an increase in turbulent kinetic energy above the long-term average during bursting times; this is shown by the curves marked β on figure 13 where we denote

$$\beta = \lim_{T \rightarrow \infty} \frac{1}{T} \int_0^T \alpha_B u^2(t; y) dt \bigg/ \lim_{T \rightarrow \infty} \frac{1}{T} \int_0^T u^2(t; y) dt.$$

Since $\gamma < \beta < \alpha$, on figure 13, we observe a rise in total turbulent kinetic energy but a lesser rise than in turbulence production rate during bursting times. Bursts are thus 'moments of relatively organized motion'.

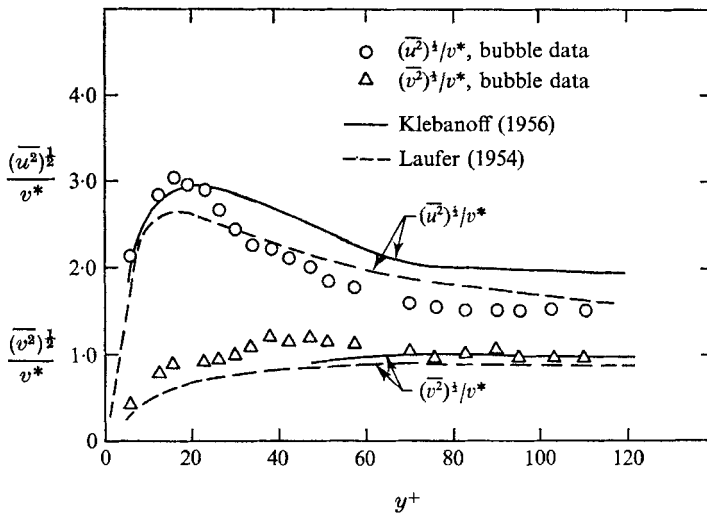


FIGURE 17. Comparison of r.m.s. fluctuation velocities, $(\overline{u^2})^{1/2}$, $(\overline{v^2})^{1/2}$, from bubble data with results of Klebanoff (1956) and Laufer (1954).

Figure 17 shows $(\overline{u^2})^{1/2}/v^*$ and $(\overline{v^2})^{1/2}/v^*$ mean-square fluctuating velocities plotted against y^+ . The figures include comparison with the data of Kelbanoff (1956) and Laufer (1954). It can be seen that except for a somewhat excessive value $(\overline{u^2})^{1/2}/v^*$ in the region $10 < y^+ < 20$ and $(\overline{v^2})^{1/2}/v^*$ in the region $y^+ < 60$, there is good agreement in value, and the trends agree everywhere.

Figure 18 gives a similar comparison for the value of non-dimensional mean turbulence production rate, \hat{P} . It also shows good agreement with the Klebanoff and Laufer data except in the region $y^+ \approx 12$. Note that in the normalization used, it can be shown that (Kim *et al.* 1968*a*) that the maximum theoretical value for $\hat{P} = -(\nu/\nu^{*4}) \overline{wv} \partial \overline{U} / \partial y$ is $\frac{1}{4}$, and this occurs where $\partial \overline{U}^+ / \partial u^+ = \frac{1}{2}$. Hence

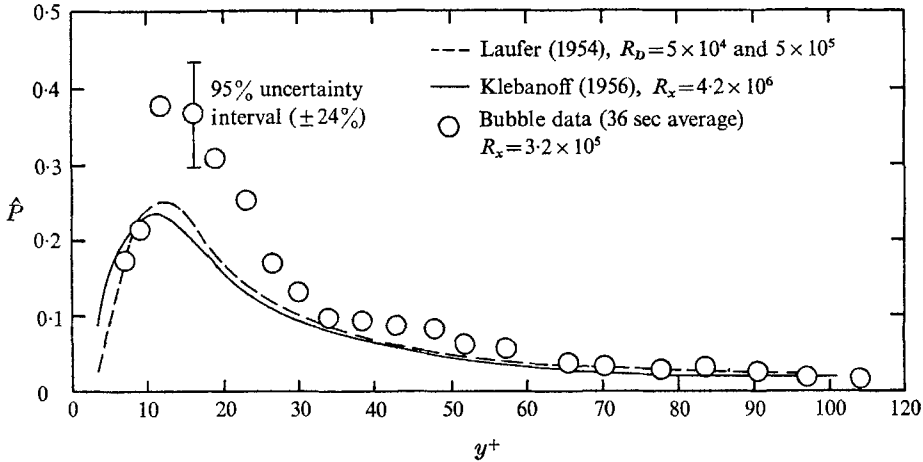


FIGURE 18. Comparison of non-dimensional turbulence production, $\hat{P}(y^+)$, from bubble data with results of Klebanoff (1956) and Laufer (1954). $\hat{P} \triangleq -(\nu/\nu^{*4}) \overline{wv} (\partial \overline{U} / \partial y)$.

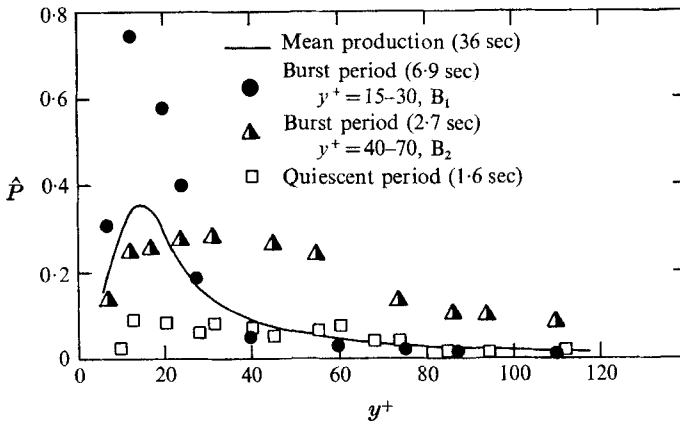


FIGURE 19. Comparison of mean values of non-dimensional turbulence production, $\hat{P}(y^+)$, with typical values for bursting times and for quiescent periods. $\hat{P} \triangleq -(\nu/\nu^{*4}) \overline{wv} (\partial \overline{U} / \partial y)$.

it is clear that an excessive value was measured in the zone near the peak in the present results. As is shown by Kim *et al.* (1968*a*), this is due to the sampling problems which are most severe just in this region owing to a combination of circumstances. Fortunately, this does not distort the main result, that is the value of α , since the α is normalized using the production for the same record.

Figure 19 compares the mean turbulence production curve from the present data with production rate during two bursting times and an apparent non-bursting period; the data points marked B₁ are for a record during the oscillatory

growth phase covering the zone $y^+ = 15-30$; those marked B_2 are for a record taken during an oscillatory growth phase in the region $y^+ = 40-70$. The term 'apparent' is used to modify the non-bursting time because there is no guarantee, with the techniques employed, that crosswise contamination from another burst (not made visible by marking fluid) is entirely absent. Presence of such an effect would tend to make the production rate too high; so that if the non-bursting curve is in error it is too high, not too low. As can be seen, the value of the production rate rises considerably in the zone where oscillatory growth is observed, but not elsewhere. Figure 20 compares the root-mean-square fluctuation

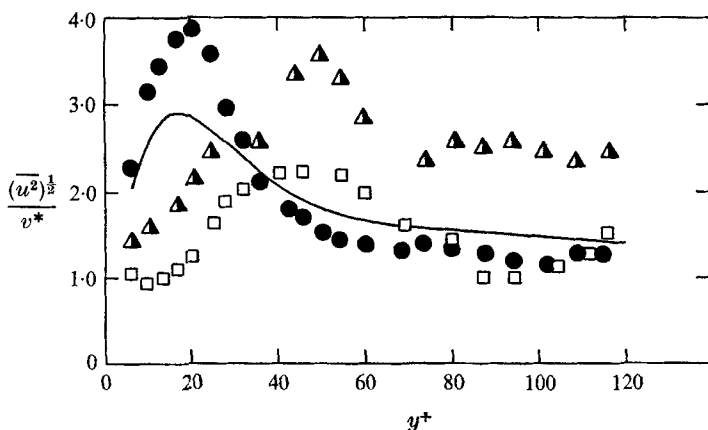


FIGURE 20. Comparison of mean values of streamwise r.m.s. fluctuation velocity, $(\overline{u^2})^{1/2}/v^*$, with typical values for bursting times and for quiescent periods. Symbols same as figure 19.

values $(\overline{u^2})^{1/2}/v^*$ with the observed values during bursting and non-bursting time periods the same as those shown in figure 19. Again, the value of the fluctuations rises considerably in the zone where oscillatory growth is observed, but not elsewhere. All of this is entirely consistent with the picture of the turbulence production as being primarily associated with a local dynamic intermittent instability, with the energy transfer concentrated primarily in the part of the motions which we have called 'oscillatory growth'. We hasten to add that this is not conclusively proved. The data on α in figure 13 do conclusively prove that essentially all the turbulence is produced during the total bursting time for the cases studied; however, the difficulties which presented running the bubble wire and hot wire simultaneously also prevented us from dissecting the details further with positive assurance. However, the various evidence in figures 14, 16, 19 and 20 strongly suggests to us that the primary energy transfer to the large disturbances does occur in the oscillatory growth stage, and that breakup is the beginning of the 'cascade' processes which make smaller fluctuations, and lead ultimately to dissipation. Whether similar processes occur in other flow situations is entirely unknown as yet, and we caution the reader against too great extrapolation, since we already know the situation is somewhat different for rough walls.

The last type of data concerns the auto-correlations of the fluctuations, and the association of them with characteristic signatures on the hot-wire traces of

the 'bursting' process. The auto-correlations for the two flows are shown in figures 21(a) and 22(a). Visual counts of bursting times are also indicated. As already noted the time between bursts, at least at these low unit Reynolds numbers, is greater than all other time scales in the flow; it is indeed distinct from the characteristic time scales of the turbulent kinetic energy of the background fluctuations. This separation in time scales again suggests a separate process controlled by some dynamics not directly associated with the general background turbulence even though perhaps affected by it. It is noted that most previous observers of auto-correlations have run to lag times, roughly around the point marked τ_s on figure 21(a). This is an entirely natural thing to do since big lag times mean big costs for data and processing times. Moreover, if one examines the auto-correlation from $\tau = 0$ to τ_s , one would erroneously believe that all interesting results were in hand at the point where $\tau = \tau_s$, and therefore logically

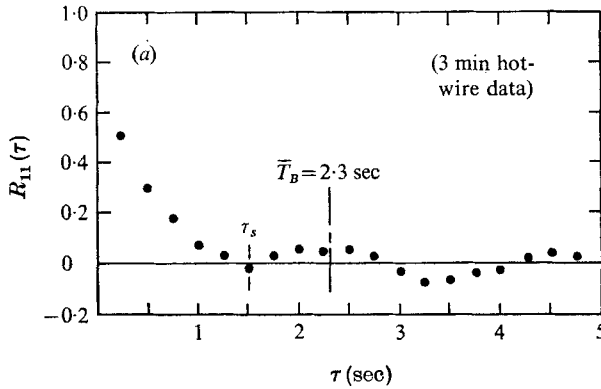


FIGURE 21(a). Auto-correlation coefficient, $R_{11}(\tau)$. 3 mm hot-wire data, $U_\infty = 0.5$ ft/sec, $y^+ = 18$.

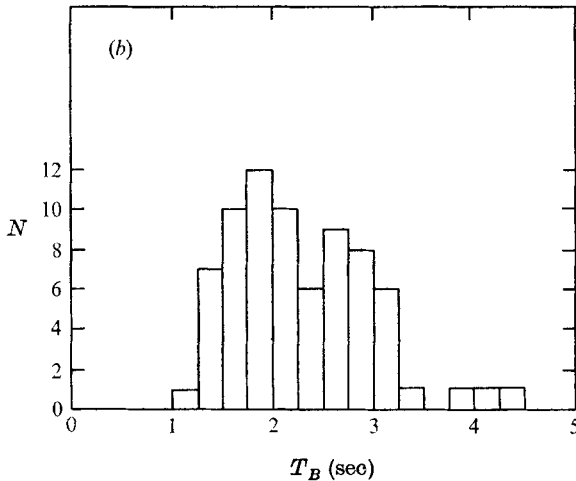


FIGURE 21(b). Histogram of time interval between bursts, $N(T_B)$. $U_\infty = 0.5$ ft/sec, H_2 bubble data. (3.5 min motion picture data.) $\sigma = 0.71$ sec, $\bar{T}_B = 2.27 \pm 0.16$ sec (20:1 odds).

shut off the analyzer or computer. This was indeed what was done in the otherwise excellent results of Bakewell & Lumley (1967) which are certainly the most extensive correlations measurements very close to the wall so far available. Indeed, the writers made the same mistake initially, but were saved by the co-existence of visual data on bursting which suggested phenomena existed at higher lag times, τ , and this was borne out by making subsequent computer runs to higher values of τ .

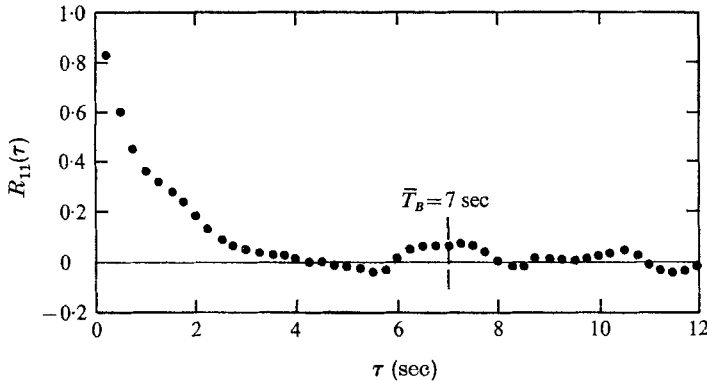


FIGURE 22(a). Auto-correlation coefficient, $R_{11}(\tau)$. 3.5 min hot-wire data, $U_\infty = 0.25$ ft/sec, $y^+ = 14$.

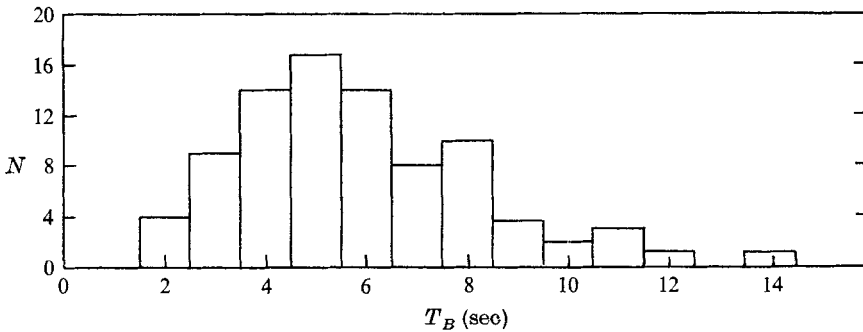


FIGURE 22(b). Histogram of time interval between bursts, $N(T_B)$. H_2 bubble data, $U_\infty = 0.25$ ft/sec. (10 min motion picture data.) $\sigma = 3$ sec, $\bar{T}_B = 6.5 \pm 0.6$ sec (20:1 odds).

Figures 21 (b) and 22 (b) show histograms of the time between bursts from visual data for the two flows. As already noted, the standard deviation about the mean value is quite large. The combination of this high standard deviation and the fact that the time between bursts is the longest time scale in the processes together create the sampling problem already discussed. However, in both figures 21 and 22 the mean value of T_B from visual data agrees with the long-time auto-correlation re-rise maximum to within the estimated uncertainty.

Figure 23 shows a comparison of the results from the visual and auto-correlation data of the present study with the visual and statistical counts of bursting frequency from the studies of Runstadler *et al.* (1963) and of Schraub & Kline (1965). The agreement in both slope and value indicates that the observed

bursting which is here associated with production is the same process observed as bursting by earlier workers. The theory of Black (1966) also suggests the same trend of variation as that shown in figures 23 and 2. However, if one extrapolates the curve of figure 23 two decades to the value of Reynolds number in the velocity fluctuation data of Willmarth & Tu (1966), a discrepancy of one order of magnitude is found. Initially, the reason for the deviation of the correlation from the data of Willmarth & Tu was not understood. It appears now, however, that the explanation lies in a dependence of F on momentum thickness Reynolds number, R_θ . This explanation has been advanced by Rao *et al.* (1969, 1971). In

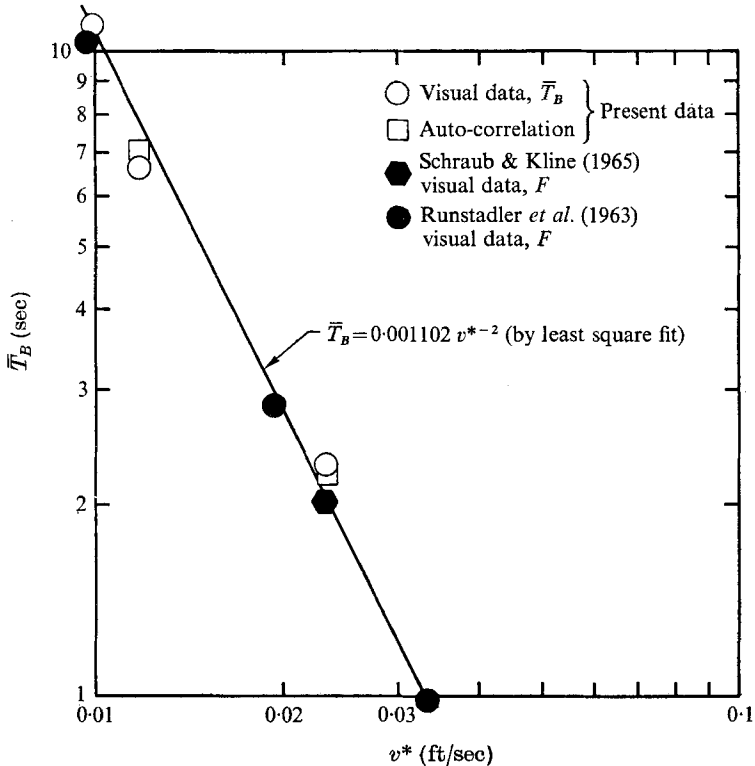


FIGURE 23. Dependence of mean time between bursts, \bar{T}_B , on friction velocity v^* for flat plate flow and moderate, nearly constant R_θ .

the experiments of Rao *et al.* the time between bursts was taken from hot-wire data (after differentiating the trace of $u(t)$ in order to make bursts stand out more clearly). The present writers believe that this technique will show the same phenomena as that which we call 'oscillatory motion', stage (2) of bursting in the visual data, but there is a need to check this technique directly against a visual study to ensure that the data are truly related as Rao *et al.* suggest and we believe. The central results of Rao *et al.* are shown on figure 24(a) and (b). Figure 24 shows two things: (i) the results are consistent with those of figure 23; (ii) figure 23 by itself is misleading owing to the fact the small variation in R_θ over the total data of figure 23 does not disclose the R_θ dependence because the effect is decreased by simultaneous variation in v^* . However, with the addition of

the data of Rao *et al.* the data of Willmarth & Tu can be reconciled with the other data sets of figure 23 as shown on figure 24.

If we accept the correlation of figure 24 as correct, then it follows that F is scaled by the outer-layer variables as opposed to λ which is scaled on inner-layer variables. We believe that these scalings are appropriate for the reasons that follow, and were indeed somewhat disturbed by the implication of figure 23 which suggests that F should be scaled by inner-layer variables since such a scaling would contravene our present physical understanding. The bubble data suggests that low-speed-streak lifting is triggered by large disturbances already present in the flow, and hence that the frequency should scale on outer variables. On the other hand, we believe the low-speed streaks arise as the highly selective response of the inner layers to a large spectrum of outer layer disturbances. See I and Sternberg (1962).

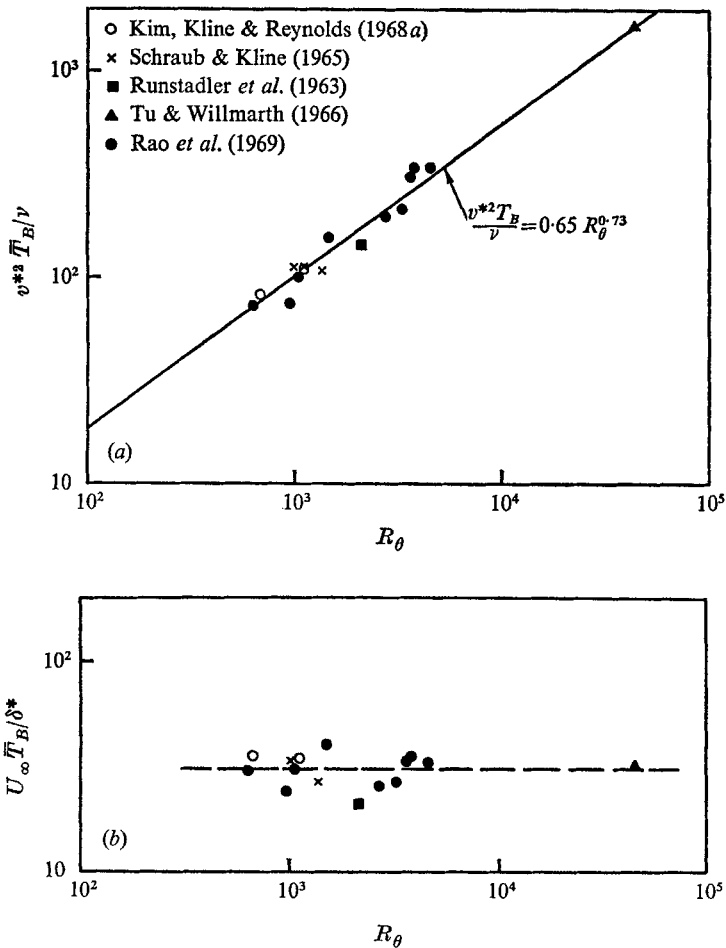


FIGURE 24. Scaling of burst frequency with R_θ . (a) Dependence of mean time interval between bursts scaled on inner variables, $v^{*2} \bar{T}_B / \nu$, on R_θ . (b) Mean time interval between bursts, \bar{T}_B , scaled on outer variables, $U_\infty \bar{T}_B / \delta^*$, versus R_θ .

Some workers have suggested that λ should also scale on outer variables. However, there are as yet no data that actually suggest anything other than at most a very weak dependence of λ^+ on R_θ . The available data are tabulated in table 1. It will be seen that all available data show no R_θ dependence excepting only that of Willmarth & Tu at very high R_θ . The variation in λ^+ is at most a factor of two, unlike that in F^+ which varies an order of magnitude over the same range of R_θ . Although more data are needed, at high R_θ , it seems reasonable to assume for the present that λ^+ is at most a very weak function of R_θ .

Finally one other important implication of the bubble data should be mentioned. The data suggest that the processes during oscillatory growth are qualitatively quite different from the processes during non-bursting times. This notion is borne out by the quantitative comparisons of u , v , uv and P during bursting and non-bursting times as seen in figures 11 to 20. Also the processes during the oscillatory motion stage are sharply intermittent and have the appearance of an organized oscillation or 'wave packet'. Thus a wave description of the turbulent shear and production may be useful. This idea of a wave description has been explored by several workers in recent years (e.g. Landahl 1967; Phillips 1967; Hussain & Reynolds 1970). None of these theories appear to be in a satisfactory final form at present, however. What is suggested here is that a two-part or dual description of the total motion, modelling the organized part as waves, and the unorganized as 'eddies' or some kind of noise, may be more appropriate than either alone. Such a dual description has in fact been carried out by Lahey & Kline (1971). Success in relating all kinds of correlation data for a variety of turbulent flows available in the literature has been achieved. This work is the subject of a separate publication now under preparation.

6. Conclusions

Detailed studies using combined-time-streak markers of hydrogen bubbles have been made to obtain instantaneous velocity profile data and overall pictures of the details of turbulence production in a boundary layer near smooth walls. Related hot-wire studies have provided turbulence production, auto-correlation, and energy spectrum data.

The quantitative data establish, for the cases studied, that essentially all the turbulence production occurs during bursting times in the zone $0 < y^+ < 100$. The qualitative data show that the bursting process can be described as made up of three stages: (i) lifting of the low-speed streaks from the innermost layer, this forms unstable (inflexional) instantaneous velocity profiles; (ii) growth of an oscillatory motion in the region of flow following from the inflexional zone; (iii) breakup of the oscillatory but well-defined motion into more random or chaotic motions accompanied by a return to the wall of the low-speed streak, and a more quiescent flow. The third stage also shows velocity profiles more nearly those of the mean profile, thus completing the cycle. This cycle is intermittent, but has a well-defined mean frequency. This much seems firmly established.

A number of other data are given; these include short duration spectra, auto-correlation data, visual signatures of hot-wire traces during bursting, comparison

of the distribution of oscillatory growth and turbulence production data of others in y^+ space, and the comparison of calculated unstable frequencies of the instantaneous profile with measured oscillatory growth frequencies. All these data suggest, but do not prove, a picture of the processes which associate the primary energy transfer from the mean flow to the fluctuations with the oscillatory growth stage of the observed flow model, and the breakup stage with the beginnings of the cascade processes leading to smaller eddies and dissipation. The data also suggest that the primary energy transfer occurs as the result of a local intermittent instability, which has a definite preferred range of frequencies of occurrence and of oscillation. This in turn suggests that a wave description of the actual process of production may be useful. This then suggests, as do the data on fluctuations, Reynolds stress, and production, that the structure of the boundary-layer shear flow may well be better described as a two-part model than as one kind of 'average eddy structure'. Considerable success in constructing such a mathematical representation of certain structural features has already been achieved and will be reported separately (Lahey & Kline 1971).

REFERENCES

- BAKEWELL, H. P. & LUMLEY, J. L. 1967 *Phys. Fluids*, **10**, 1880.
 BLACK, T. J. 1966 *Proc. Heat Transfer and Fluid Mechanics Institute*. Stanford University Press.
 CLARK, J. A. 1968 *Trans. ASME, J. Basic Engng.* **90**, 455.
 COANTIC, M. 1967 *Proc. 4th EUROMECH. Colloq., Southampton*.
 CORINO, E. R. & BRODKEY, R. S. 1969 *J. Fluid Mech.* **37**, 1.
 EMMONS, H. W. 1951 *J. Aero. Science*, **18**, 490.
 GUPTA, A. K. 1970 Dissertation University Southern California.
 HUSSAIN, A. K. M. F. & REYNOLDS, W. C. 1970 Report FM-6, Department of Mechanical Engineering, Stanford University.
 KIM, H. T., KLINE, S. J. & REYNOLDS, W. C. 1968*a* Report MD-20, Department of Mechanical Engineering, Stanford University.
 KIM, H. T., KLINE, S. J. & REYNOLDS, W. C. 1968*b* *ASME-ESL motion picture film*, K5. Obtainable for purchase or rent from Engineering Societies Library, 345 East 47th Street, New York, N.Y. 10017.
 KLEBANOFF, P. S. 1956 *NACA TN-2178* or Report 1247.
 KLINE, S. J. 1963 *Flow Visualization*. 16 mm movie available from Eycyclopaedia Britannica Educational Corp., 425 North Michigan Avenue, Chicago, Ill. 60611.
 KLINE, S. J. 1967 *Phys. Fluids, Suppl. Kyoto Symp.*
 KLINE, S. J., REYNOLDS, W. C., SCHRAUB, F. A. & RUNSTADLER, P. W. 1967 *J. Fluid Mech.* **30**, 741.
 KLINE, S. J. & RUNSTADLER, P. W. 1959 *J. Appl. Mech. Trans. ASME*, **26**, no. 2, 166.
 LAHEY, R. T. & KLINE, S. J. 1971 Report MD-26, Department of Mechanical Engineering, Stanford University.
 LANDAHL, M. 1967 *J. Fluid Mech.* **29**, 441.
 LAUFER, J. 1954 *NACA Report 1174* or TN-2954.
 LIU, C. K., KLINE, S. J. & JOHNSTON, J. P. 1966 Report MD-15, Department of Mechanical Engineering, Stanford University.
 MEYER, K. A. & KLINE, S. J. (1962) *A Visual Study of the Flow Model in the Later Stages of Laminar-Turbulent Transition on a Flat Plate*. Report MD-7, Department of Mechanical Engineering, Stanford University.

- PHILLIPS, O. M. 1967 *J. Fluid Mech.* **27**, 131.
- RAO, K. N., NARASIMHA, R. & BADRI NARAYANAN, M. A. 1969 Report 69 FM 8, Department of Aeronautical Engineering, Indian Institute of Science, Bangalore.
- RAO, K. N., NARASIMHA, R. & BADRI NARAYANAN, M. A. 1971 *J. Fluid Mech.* **48**, 339.
- RUNSTADLER, P. W., KLINE, S. J. & REYNOLDS, W. C. 1963 *An Experimental Investigation of the Flow Structure of the Turbulent Boundary Layer*. Report MD-8, Department of Mechanical Engineering, Stanford University.
- SABIN, C. M. 1963 Report MD-9, Department of Mechanical Engineering, Department of Mechanical Engineering, Stanford University.
- SCHRAUB, F. A. & KLINE, S. J. 1965 *A Study of the Structure of the Turbulent Boundary Layer With and Without Longitudinal Pressure Gradients*. Report MD-12, Department of Mechanical Engineering, Stanford University.
- SCHRAUB *et al.* 1965 *J. Basic Engng. Trans. ASME*, **87**. (See also *ASME* preprint FE-20.)
- STERNBERG, J. 1962 *J. Fluid Mech.* **13**, 241.
- STUART, J. T. 1965 *NPL Aero. Report* 1147.
- UZKAN, T. & REYNOLDS, W. C. 1967 *J. Fluid Mech.* **28**, 803.
- WILLMARTH, W. W. & TU, B. J. 1966 University of Michigan Report no. 02920-3-T.

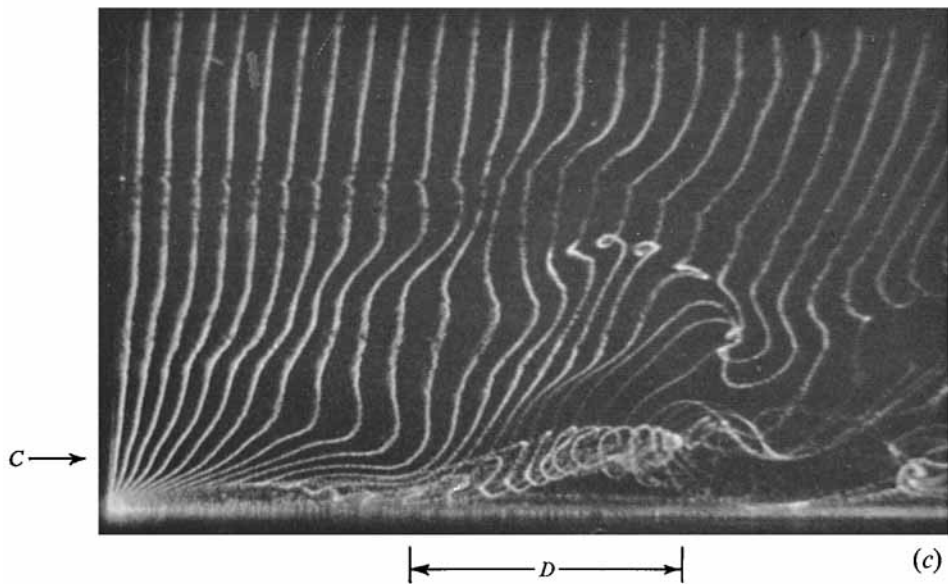
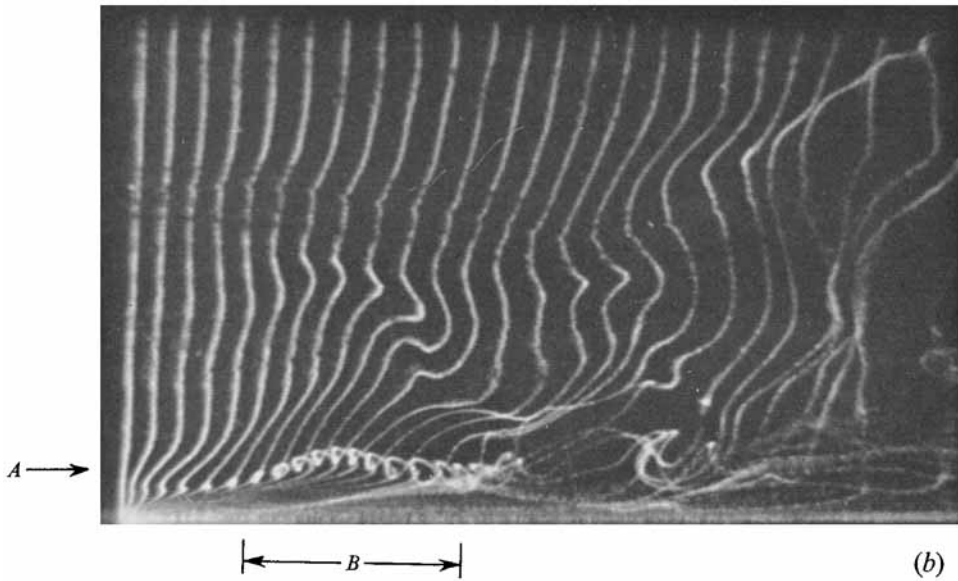


FIGURE 8 (*b*), (*c*). Photographic illustrations of H_2 bubble time lines showing formation of a typical streamwise vortex motion during second stage of bursting. (*b*) Streamwise vortex formation in buffer region. The vortex extends from line *A* over zone *B*. Note also inflexional profile near normal wire. (*c*) Development of the vortex downstream. Notice the radius of rotation growing as the flow proceeds downstream. A portion of vortex along line through *C* over zone *D* is the same as shown in (*b*), 0.5 sec earlier.

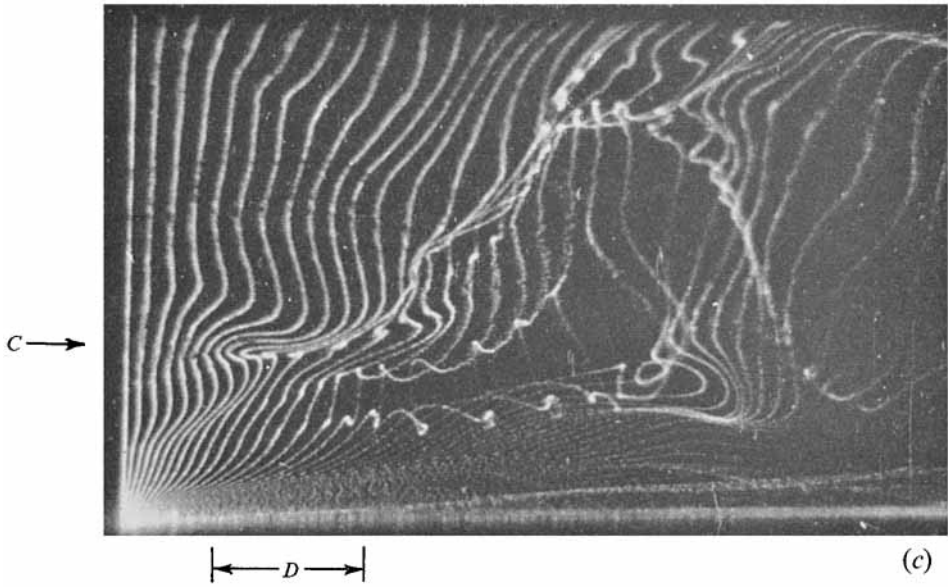
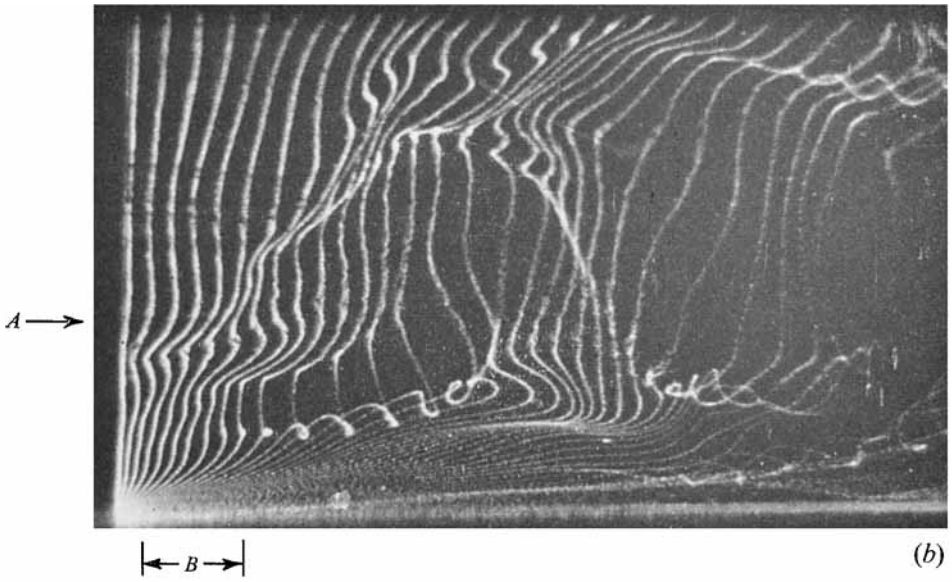


FIGURE 9(b), (c).

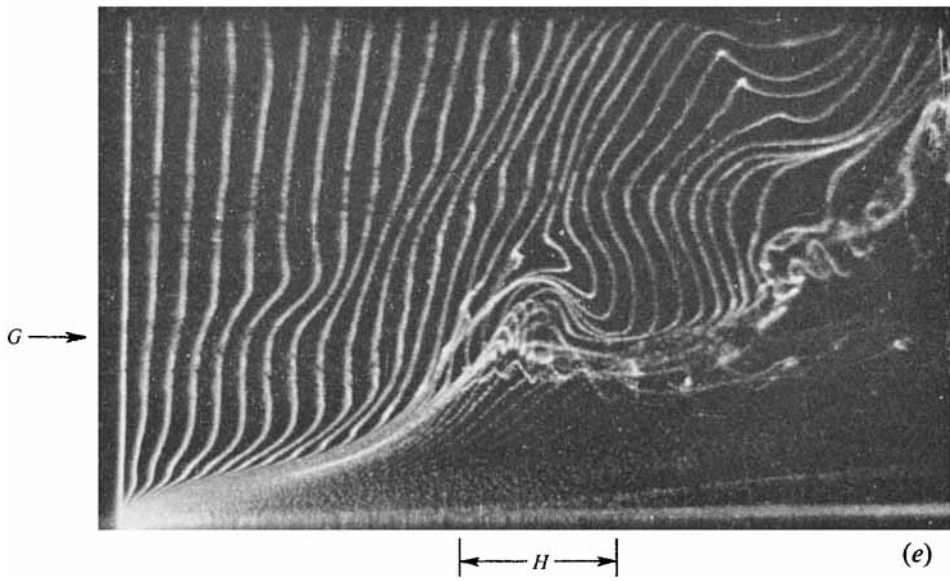
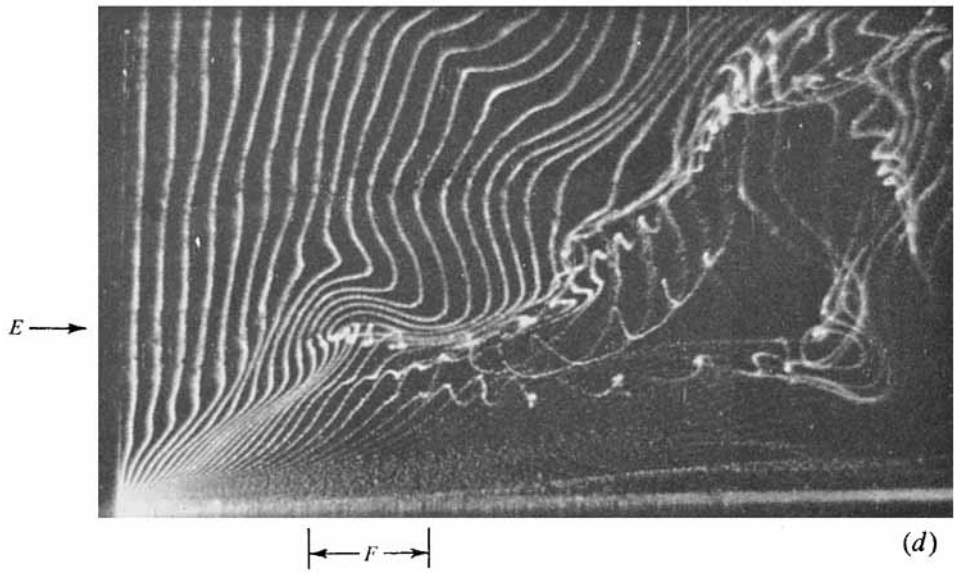


FIGURE 9(d), (e).

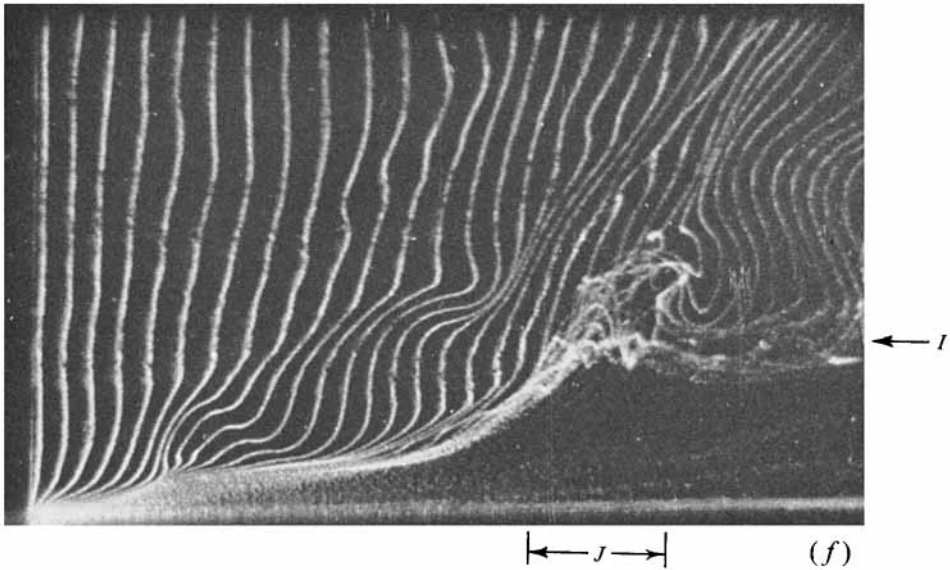


FIGURE 9(b)-(f). Photographic illustrations of H_2 bubbles showing formation and break-up of a typical transverse vortex motion during bursting. (b) Inflexional profile near intersection of line through *A* with zone *B*. $t = t_0$. (c) Kinked time lines near the intersection of line through *C* with zone *D*. This is incipient formation of transverse vortex. $t = t_0 + 0.37$ sec. (d) Formation of transverse vortex near the intersection of line *E* with zone *F* and line *G* with zone *H*. $t = t_0 + 0.74$ sec. (e) Formation of transverse vortex near the intersection of line *E* with zone *F* and line *G* with zone *H*. $t = t_0 + 0.12$ sec. (f) Breakup following the transverse vortex near the intersection of line *I* with zone *J*. $t = t_0 + 1.67$ sec.

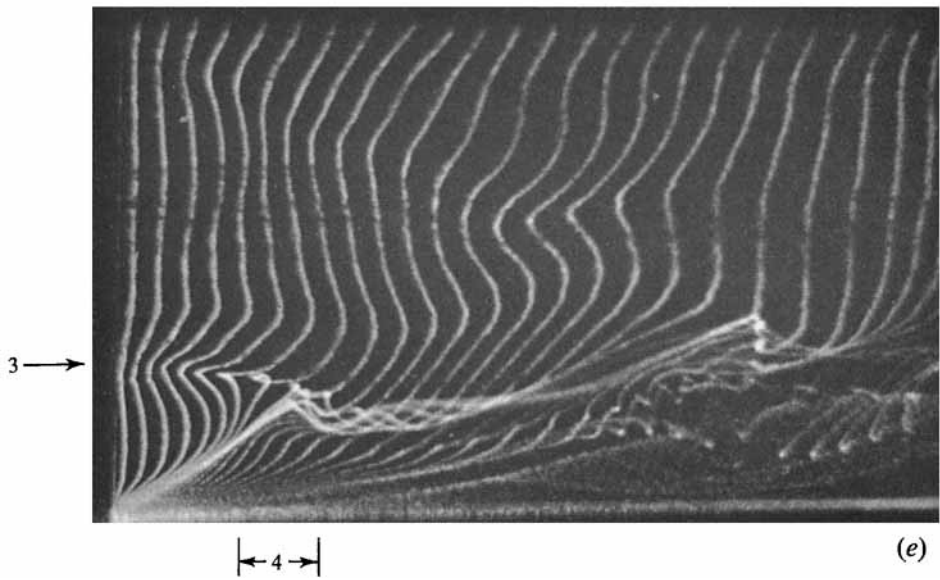
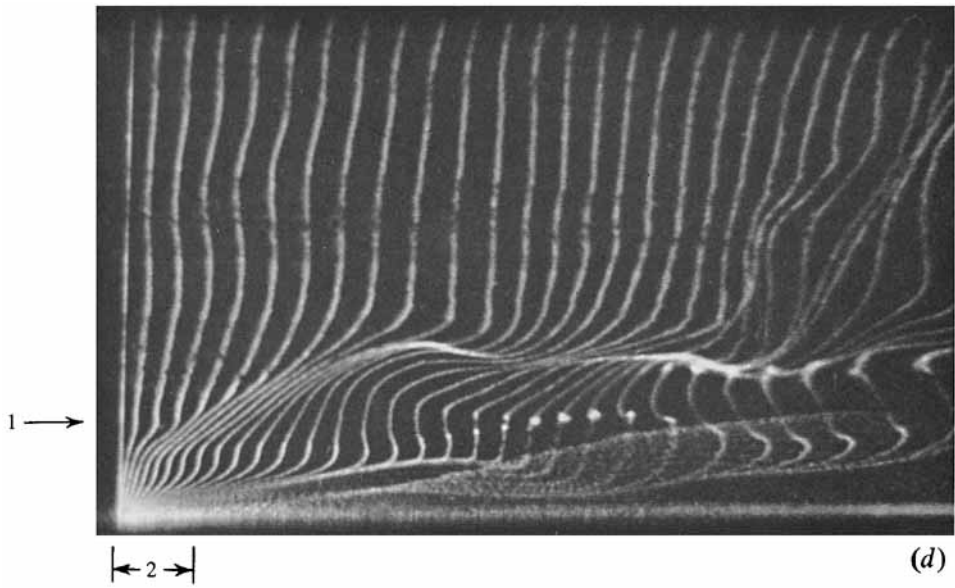


FIGURE 10(*d*), (*e*).

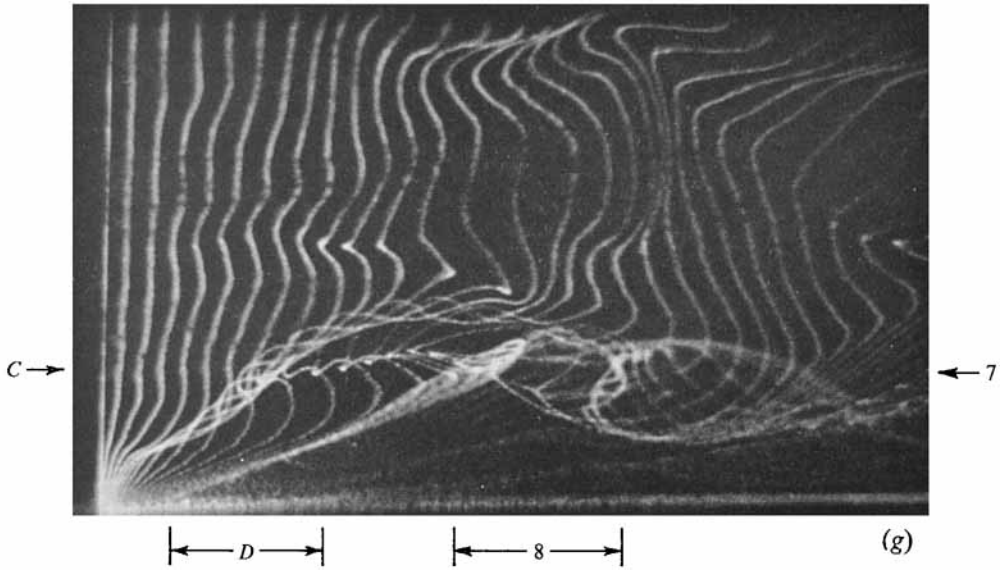
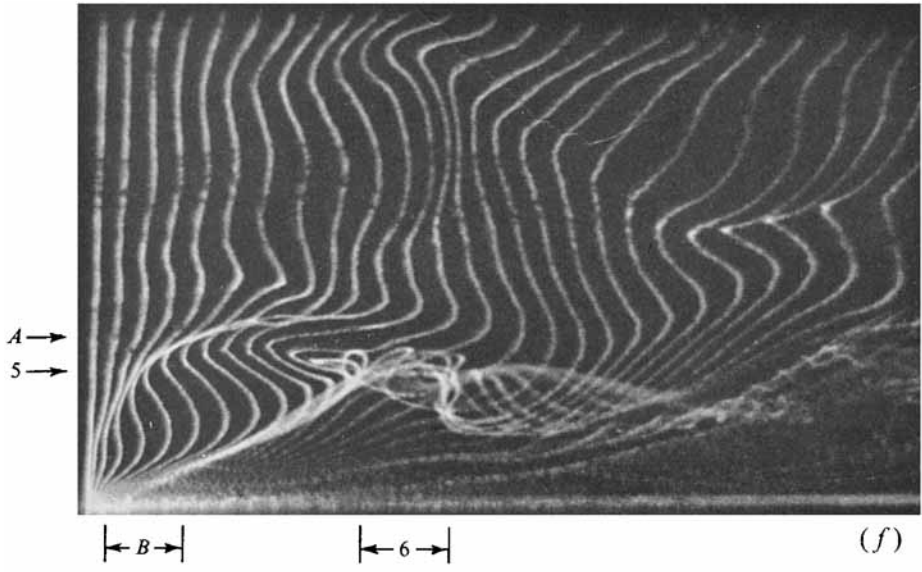


FIGURE 10(*f*), (*g*).

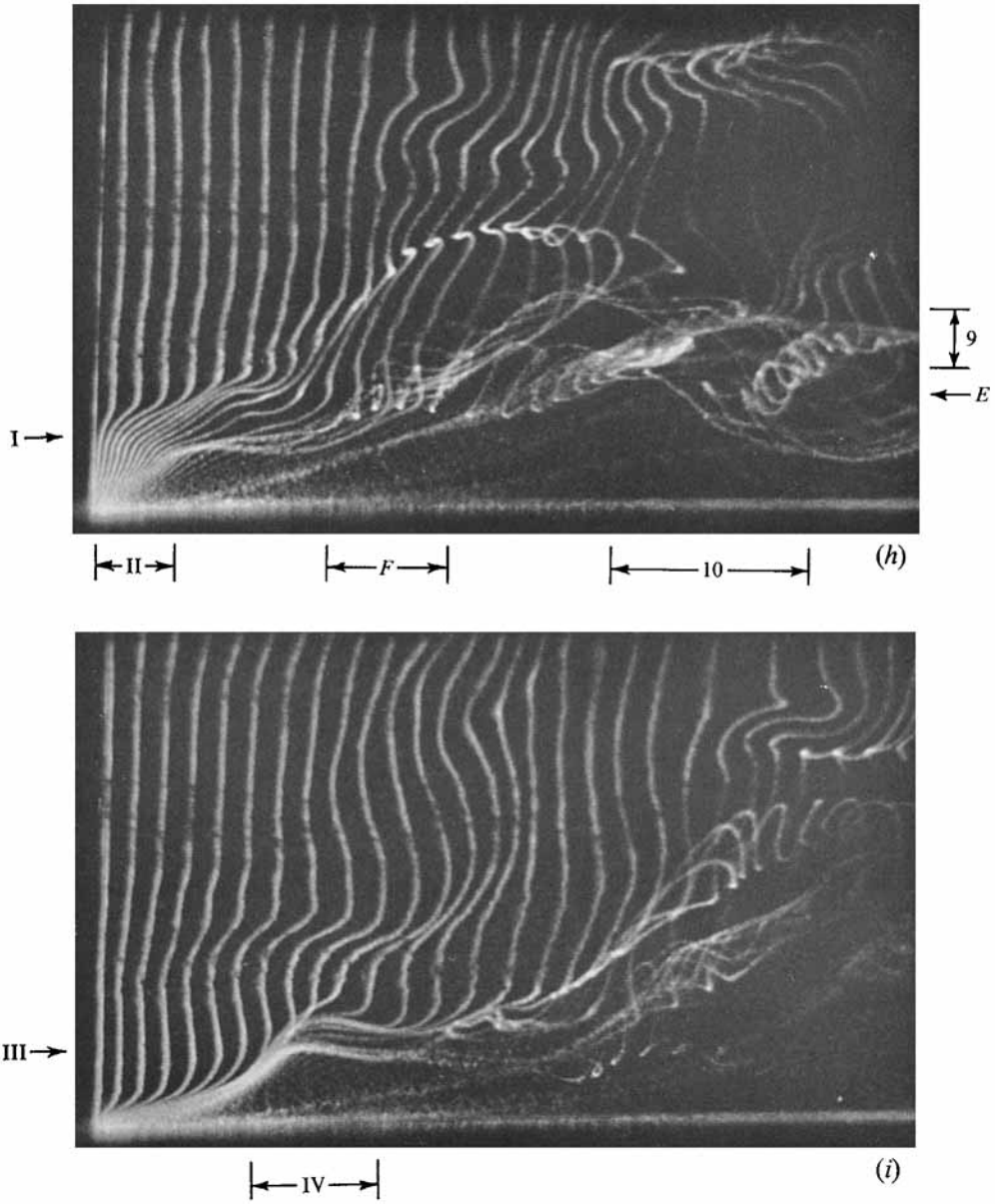


FIGURE 10(h), (i).

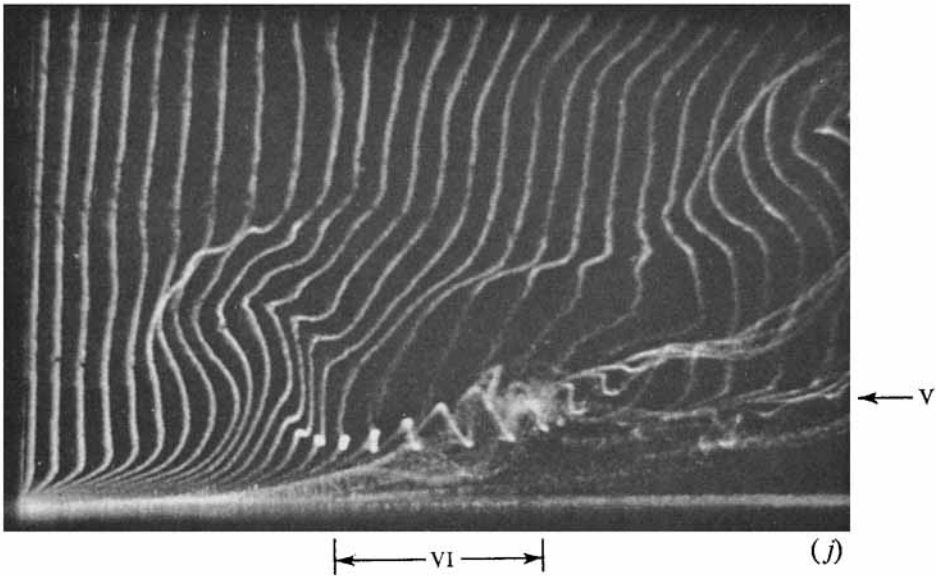


FIGURE 10(*d*)–(*j*). Photographic illustrations of H_2 bubbles showing formation of a typical ‘wavy mode’ second stage of bursting. (*d*) $t = t_0$. (*e*) $t = t_0 + 0.65$ sec. (*f*) $t = t_0 + 1.07$ sec. (*g*) $t = t_0 + 1.44$ sec. (*h*) $t = t_0 + 1.86$ sec. (*i*) $t = t_0 + 2.51$ sec. (*j*) $t = t_0 + 3.3$ sec.